2012-12-13

A Matlab Model of a 1.6 Liter Engine with Experimental Verification

Patrick Seemann
University of Miami, p.s.seemann@gmail.com

UNIVERSITY OF MIAMI

A MATLAB MODEL OF A 1.6 LITER ENGINE WITH EXPERIMENTAL VERIFICATION

By

Patrick Shannon Seemann

A DISSERTATION

Submitted to the Faculty
of the University of Miami
in partial fulfillment of the requirements for
the degree of Doctor of Philosophy

Coral Gables, Florida

December 2012

UNIVERSITY OF MIAMI

A dissertation submitted in partial fulfillment of
the requirements for the degree of
Doctor of Philosophy

A MATLAB MODEL OF A 1.6 LITER ENGINE WITH EXPERIMENTAL VERIFICATION

Patrick Seemann

Approved:

_____
Michael R. Swain, Ph.D.
Associate Professor
Mechanical & Aerospace Engineering

_____
M. Brian Blake, Ph.D.
Dean of the Graduate School

_____
Paul M. Bevilaqua, Ph.D.
Professor
Mechanical & Aerospace Engineering

_____
Singiresu S. Rao, Ph.D.
Professor
Mechanical & Aerospace Engineering

_____
Matthew R. Swain, Ph.D.
President
Analytical Technologies Incorporated
Miami, Florida

SEEMANN, PATRICK (Ph.D., Mechanical Engineering)

A Matlab Model of a 1.6 Liter Engine with Experimental Verification (December 2012)

Abstract of a dissertation at the University of Miami.

Dissertation supervised by Professor Michael R. Swain.
No. of pages in text. (66)

Many different models exist for internal combustion engines. When designing and optimizing an internal combustion oftentimes key parameters are missing. Commonly no Pressure-Volume diagrams exist. It is the purpose of this dissertation to prove that a simple and accurate model can generate excellent results. The results of the model were verified using three different engine configurations and found to give accurate results for power and BTE. These theoretical results helped to better understand each engine configuration. The three engine configurations varied in swirl and squish. The engine configurations were all tested using propane as a fuel.

The three engine configurations were based on the same engine with different cylinder heads. The engine was specifically developed for generator usage in the 15-17kW range. The engine was based on a 1.6L four cylinder engine. The engine was configured for low RPM operation, propane as a fuel, minimal friction and ease of data acquisition. The different cylinder heads had varying squish and swirl in order to better understand their relation to BTE. Of the three configurations tested the Super High Swirl engine configuration had a maximum BTE of 37.5%. This Air-Fuel ratio used was

λ=1.66. This engine configuration had 33.9% squish, an average swirl ratio of 3.2 and a compression ratio of 12.7:1. The model was able to capture excellent results between the experimental and theoretical model. The theoretical model was able to capture the additional heat losses from the increased gas velocities associated with squish and swirl, without modifying the heat loss coefficient for each configuration and data set to match experimental results.

Acknowledgement

I would like to thank Dr. Michael Swain. Without his help my undergraduate, Master's or this Ph.D. would not have been possible. I would also like to thank Dr. Matthew Swain for his help with setting up the Matlab models for this thesis.

My parents have provided me the inspiration and support to always do my best. I would like to thank my parents.

I would like to thank my girlfriend Elizabeth Gormley for all her support.

Table of Contents

List of Figures

List of Tables

Definitions

BDC= Bottom Dead Center

BTE= Brake Thermal Efficiency

BMEP= Brake Mean Effective Pressure

C= Coefficient for Mass Lost by Blow-by

CR= Compression Ratio

c_p= Specific Heat at constant pressure

Genset= Generator Set

H= Enthalpy

h= Heat transfer coefficient

IMEP= Indicated Mean Effective Pressure

ITE= Indicated Thermal Efficiency

L= Rod Length

L_{MAX}= Max Lift

m= Mass

P= Pressure

p_m=Manifold Pressure

Q= Energy Transferred as Heat

S= Stroke Length

SOHC= Single Overhead Cam

T= Temperature

TDC= Top Dead Center

u= Specific Energy

V= Volume of Combustion Chamber

VD= Valve Open Duration

VO= Valve Opening

V_p= Instantaneous Piston Speed

v= Specific Volume

x= Mole Fraction of Burned Gasses

Z= Mach Index Number

$\epsilon=\frac{S}{2L}$= Half Stroke to Rod Ratio

θ= Crank Angle

ϕ= Equivalence Ratio

ω= Rate of Angular Rotation

Chapter 1 Introduction

The need for electricity spans the globe; access via a power grid can be limited and sometimes interrupted. In these cases gensets are utilized to provide electricity. The fuel for these gensets can vary but because it is highly portable and is stable during long term storage LPG has proven to be one of the principal fuels for gensets. This work describes the design of a high efficiency LPG fueled engine for a 15 to 17 kW electric output genset. The size of the genset was chosen to be consistent with the class II EPA requirements dictated in 40 CFR part 90. The requirements limit genset engine output to 19 kW. Present gensets utilize automobile engines which are designed to operate on gasoline at engine speeds exceeding 6000 RPM with air fuel ratios of λ=1.0. The use of LPG in a genset engine produces different design constraints than those for automotive applications. The three most influential constraints are as follows:

1. The original gasoline powered engine is designed with a great deal of excess breathing capability because of its expected high RPM operation.
2. It is designed to operate with a fuel of much lower octane number than LPG.
3. Stoichiometric gasoline has a much higher flame speed than lean LPG mixtures produce.

This work recognizes that the engine designed for gasoline operation is ill-suited for operation with LPG. The solution is to redesign the engine. Since redesign of the engine requires multiple new components. Cost reduction considerations make it appropriate to rebuild a used engine to meet the requirements of a new design. Rather than rebuild a more costly new engine. It should be noted that the design process described herein paid close attention to improved light load efficiency. This is because the startup current draw

for a compressor is much higher than the steady state operating current draw. Consequently a genset cannot operate continually at high load because it would not have adequate reserve power to start the compressor in an air conditioner or refrigerator.

Other research efforts (Quader, 1974), (Li, 2002), (Mizushima et al., 2009) have improved the efficiency of automobile engines fueled with LPG. They utilized replacement components to increase compression ratio and employed fuel injection to deliver the desired air-fuel mixture to multiple cylinders. The work effort utilized a low pressure venture gas mixer to deliver fuel to a pre-chamber in the intake manifold. The variation in cylinder to cylinder air-fuel ratio was as small as any fuel injection system with much lower component cost. The efficiency of the engines developed herein was superior to that of the other research efforts. This improvement occurred despite the disadvantage of the use of a smaller 400 cc/cylinder engine in this effort as opposed to 500 cc/cylinder and 660 cc/cylinder of the other efforts.

Three approaches were used to improve engine fuel efficiency. They are as follows. First the engine frictional losses were reduced by redesigning crankshaft bearing, oil pump, and valve train components. This was done by taking advantage of the 1800 RPM operational speed of the genset. For the B series SOHC two valve Mazda 1.6L engine chosen, the original operational engine speed was 5500 RPM leaving the original gasoline fueled engine designed for much higher internal inertial forces. The second fundamental modification was to increase the compression ratio to take advantage of LPG's higher octane. Work initiated with a 12.2:1 compression ratio which is LPG's critical compression ratio (Ferguson, C. 1986, pg 437), (Obert, E. 1973, pg 235). Data analysis showed this could be raised to 12.7:1 to produce further increased thermal

efficiency. The third fundamental modification was optimization of swirl ratio and squish area while minimizing combustion chamber surface to volume ratio. This was done to mitigate the reduction in thermal efficiency caused by the low flame speed of lean LPG air-fuel mixtures. Lean mixtures were used to produce a high ratio of specific heats of the working fluid. Flame speed enhancement via swirl and squish was used because the only cost is CNC reforming of the combustion chamber.

The hypothesis that the previous modification could produce large increases in thermal efficiency was tested by constructing and testing examples of modified engines. The thermal efficiencies of the modified engines were compared with the thermal efficiencies of the original 1.6 L Mazda engine fueled with LPG. The original rebuilt B-Series SOHC two valve Mazda engine produced 29.4% BTE at 115 N*m of torque, 28.5% BTE at 98 N*m and 23.2% BTE at 41 N*m. The low cost rebuilt engine derived here produced 37.2% BTE at 98 N*m of torque, 37.5% BTE at 89 N*m and 31.1% BTE at 41 N*m.

The thesis first describes the design methodology and then the Matlab one-dimensional thermodynamic computer model of the engine cycle that was used to aid in the design process. The model uses the first law of thermodynamics generating an ODE to determine pressure rise in the internal combustion engine. The model was separated into five segments to model the engine cycle. The five segments are intake, compression, combustion, expansion and exhaust. They can be seen in the Pressure-Volume diagram. Following the model description the analysis of the data by the model is presented. Following that is the description of the experimental setup, results and conclusions.

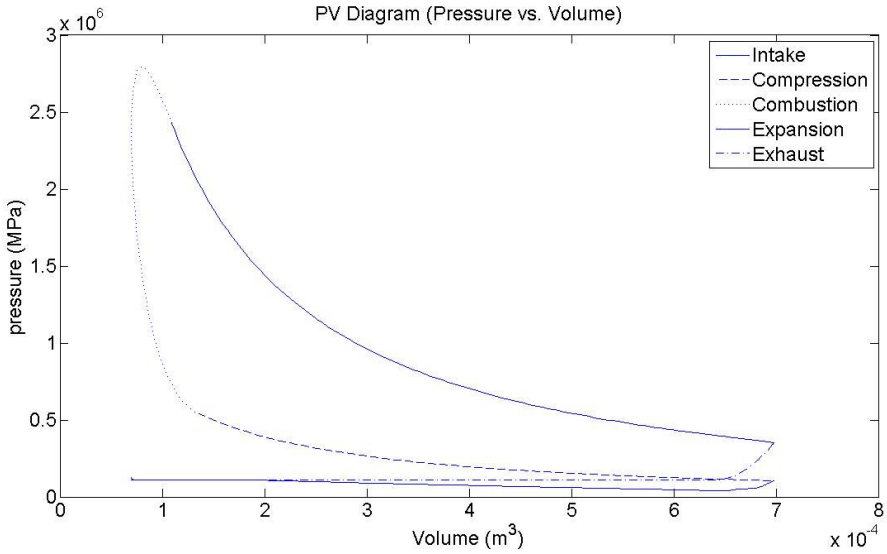

Figure 1- Pressure Volume Diagram

Chapter 2 Experimental Engine Design Methodology

A number of businesses, both large and small, manufacture LPG powered electrical generator sets (gensets). The gensets are used within the United States and exported for use overseas. They are used to generate electricity in emergencies and for off-grid locations. The internal combustion engine powering the genset is generally a mass-produced automotive engine and not specifically optimized for use in a genset. This research effort is an investigation into designing a genset engine which could be fabricated from rebuilt used automobile engines. An example of a rebuilt automobile engine which demonstrates improved efficiency over present production gensets was designed and tested. The eventual advantage to doing so would be to provide a lower cost more efficient internal combustion engine to power electrical gensets. The principal goal was to obtain the high brake thermal efficiency without utilizing potentially expensive hardware. This research effort converted an automotive 1.6 L engine for use in a genset. The original stock engine BTE at various loads while operating on LPG at λ=1.0 can be seen in Figure 2. The maximum BTE recorded for the stock engine was 29.4%. A 1 .6 L engine, suitable for 15 kW to 17 kW gensets, was constructed and tested producing brake thermal efficiencies in excess of 37%. Generators are commonly operated at low load for extended periods of time and only run at high loads during brief power surges. The emissions requirements reflect this usage. Although emissions were not explored during this experiment, most of the experimentation and modeling is concerned with low load engine requirements. A computer model specific to the engine and application was constructed to conduct thermodynamic cycle analysis. The model was constructed to provide insight into the trade-off between time losses and heat losses

using best efficiency spark advance data instead of cylinder pressure versus time data as input.

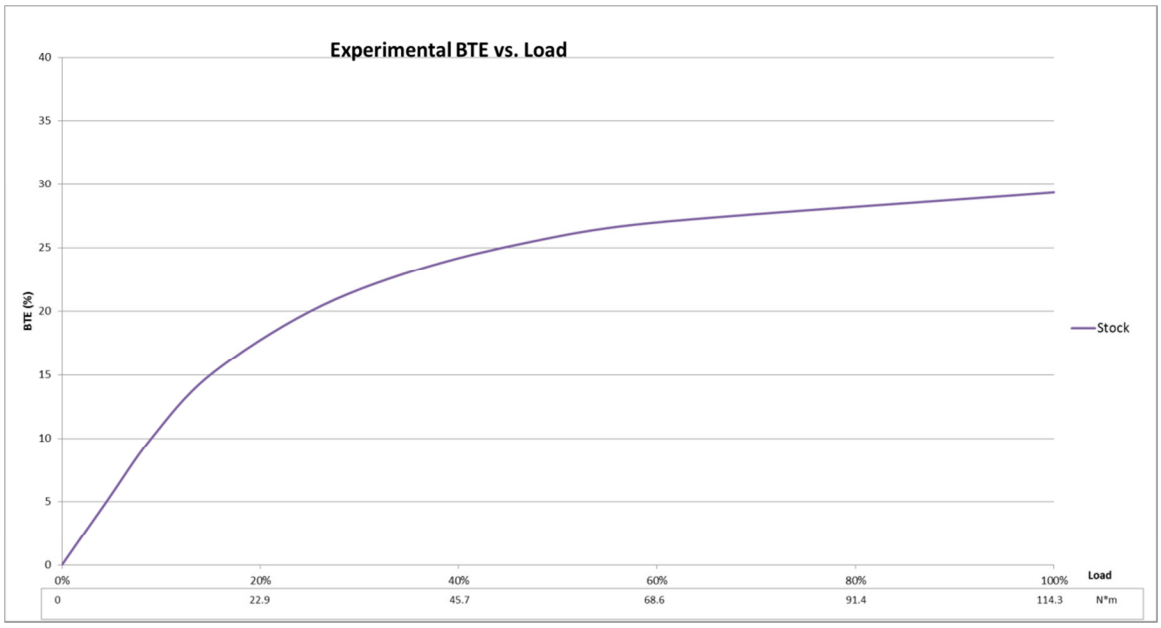

Figure 2- BTE vs. Load for Stock Engine

A simplified depiction of the Otto cycle can be represented by the following equation. It can be seen that high efficiency is related to high compression ratios and high ratios of specific heats. Compression ratio is limited by the fuel's octane and heat losses. The combustion chamber should remain compact in order to minimize the distance traveled by the flame and reduce the heat losses by using a low surface to volume ratio.

$$n = 1 - \frac{1}{CR^{(k-1)}} \quad \text{Equation 1}$$

A critical compression ratio for propane was documented as 12.2:1 (Ferguson, C. 1986, pg 437),(Obert, E. 1973, pg 235) in testing conducted by General Motors. Since increasing the compression ratio increased the surface to volume ratio, determining the proper stroke and bore to minimize the surface to volume ratio is critical. Table 1 shows

the surface to volume ratio in cm^{-1} as a function of compression ratio and stroke in mm for a 1.6L engine. The longer the stroke, the lower the surface to volume ratio. The engine tested used a stroke of 83.6 mm and bore of 79 mm. In order to increase the ratio of specific heats the temperatures of the working fluids must be minimized. Two methods are commonly employed to reduce temperatures of gasses during combustion. They are either lean mixtures or exhaust gas recirculation (EGR). For this experiment lean mixtures was chosen to reduce combustion temperatures as well as heating from exhaust gasses. Lean mixtures also reduce pumping losses by increasing manifold pressure for similar fuel flow rates.

Table 1 - Surface to Volume Ratio related to Compression Ratio and Stroke

		Compression Ratio						
		9	**10**	**11**	**12**	**13**	**14**	**15**
Stroke (mm)	**85.0**	2.12	2.33	2.55	2.77	2.99	3.22	3.44
	80.0	2.21	2.45	2.68	2.92	3.15	3.39	3.63
	75.0	2.33	2.57	2.83	3.08	3.34	3.59	3.85
	70.0	2.46	2.73	3.00	3.27	3.55	3.83	4.10
	65.0	2.61	2.90	3.20	3.50	3.80	4.10	4.40

Since the engine would be used for power generation an engine operation speed of 1800 RPM was chosen to minimize generator complexity for 60 Hz applications by eliminating the need for a gear box. In addition the relatively low speed reduces engine friction and increases generator longevity.

Low internal friction, quantified by frictional mean effective pressure (FMEP), is desirable to assist in high light load thermal efficiencies. Modifications were made to the engine to reduce FMEP. Crankshaft main bearing and journal bearing sizes were 49.9 mm diameter / 17.6 mm length and 39.9 mm diameter / 17.1 mm length respectively.

Cast iron connecting rods were 139.9 mm long and weighed 418 g. Custom forged flat top pistons were made for the 79.0 mm bore with 20 mm wrist pins and weighed 280 g including rings. The standard pistons could have been modified for use but would have required in increase in stroke. Intake and exhaust valve reliefs totaling 0.5 cc were cut into the pistons (Figure 3). Valve spring pressure was reduced 50% in the final form of the Super High Swirl engine configuration. Flat top pistons were used to aid in obtaining the desired compression ratio without increasing surface to volume ratio of the combustion chamber. The low friction ring package consisted of a 1 mm steel gas nitrated barrel face top compression ring and a 1.2 mm cast iron phosphate coated tapered face Napier scraper second ring. The three-piece oil ring was 2.8 mm wide and used a stainless steel flex vent spacer with gas nitrited rails. Additional engine information is given in the appendix section A.1.

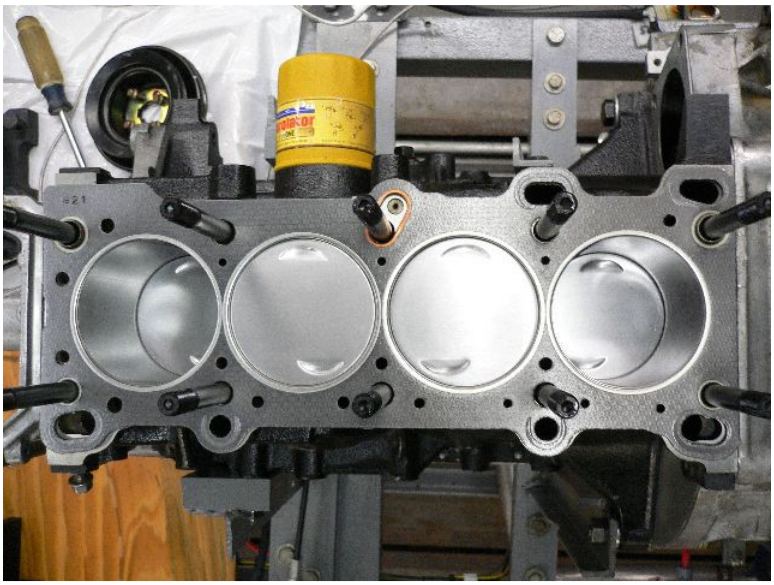

Figure 3 - Short Block with Flat Top Pistons

The piston utilized no pin offset. Oil was pressurized with a nine lobe crankshaft driven oil pump. The cylinder head selected was from a smaller 1.3 L engine. The use of

this head required repositioning the water jackets but negated the need to weld more aluminum into the combustion chamber to obtain compression ratios between 12.0:1 and 13.5:1. Of additional benefit was the intake valve head diameter of 31.75 mm and intake port diameter of 26.0 mm. The small size of the inlet system produced a Mach Index Number (Z.) of 0.20 to 0.22 at 1800 rpm and allowed for a variety of modifications to alter inlet swirl (Table 2). Table 2 shows the seven cylinder heads developed on the flow bench. Only three (IA, IVA and VD) were tested on the engine. Two different cam profiles are shown in Figure 4. The cam profile for the Super High Swirl engine was modified to close the intake valve 6° early and reduce valve overlap sufficiently to reduce residual flow into the intake manifold by 50%. The first two configurations tested used the smaller intake valves and the third configuration for Super High Swirl with the larger intake valves. The valves are shown in Figure 5 and Figure 6.

Table 2 – Cylinder Head Data

Engine Configuration	Cylinder Head	Intake Valve Diameter (cm)	Valve Shroud Angle °	Flow Rate Averaged Swirl Ratio		Intake Valve Lift (cm)			
						0.254	0.508	0.762	0.889
Engine 1 (LS)	IA	3.175	65	0.38	Swirl Ratio	0.58	0.40	0.33	0.33
					Flow Rate LPM	1308	2313	2707	2792
	IIA	3.175	70	0.66	Swirl Ratio	0.61	0.85	0.65	0.55
					Flow Rate LPM	1266	2277	2707	2789
	IIIA	3.175	75	0.89	Swirl Ratio	0.62	1.31	0.83	0.72
					Flow Rate LPM	1246	2243	2648	2724
Engine 2 (HS)	IVA	3.175	90	1.5	Swirl Ratio	2.91	2.74	0.82	0.72
					Flow Rate LPM	968	1877	2438	2602
	VB	3.429	90	2.56	Swirl Ratio	3.01	3.28	2.30	2.09
					Flow Rate LPM	1223	2093	2716	2812
	VC	3.6068	90	2.8	Swirl Ratio	4.57	3.38	2.39	2.11
					Flow Rate LPM	1034	2067	2676	2795
Engine 3 (SHS)	VD	3.7592	90	3.2	Swirl Ratio	7.16	3.69	2.49	2.30
					Flow Rate LPM	866	1934	2616	2775

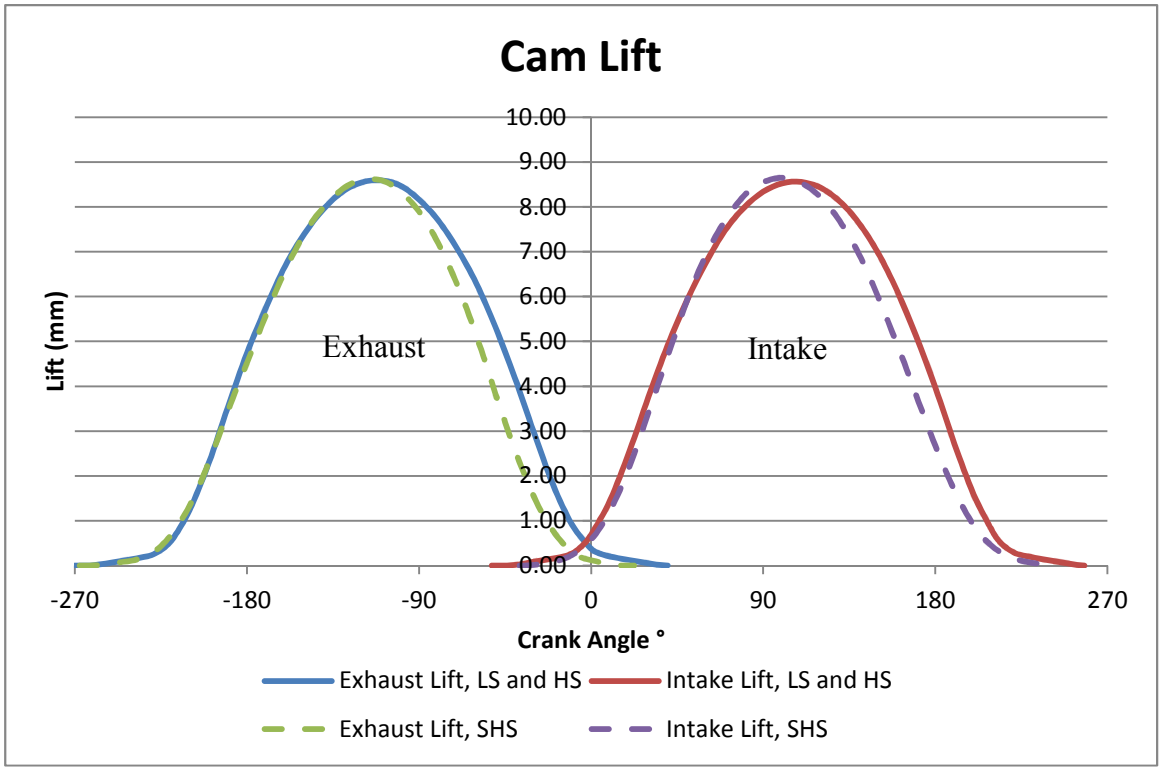

Figure 4 - Engine Cam Durations

Figure 5 – Valves, Pictured Left to right Exhaust Valve, LS and HS Intake Valve, SHS Intake Valve

Figure 6 - SHS Valves, springs and retainers

The redesign of an automotive engine for use in a genset requires additional attention to heat losses. The choice and design of the cylinder head and combustion chambers (Figure 7, Figure 8, and Figure 9) was done with attention to reduced surface area. High compression ratios and high mixture turbulence inherently increases heat losses. Lean mixtures require augmentation of mixture turbulence to increase the inherently low flame speed. The first configuration tested (IA – Low Swirl) employed a 12.2:1 compression ratio and 18.4% squish area as the principal means of increasing flame speed and reducing the lean limit of combustion. The second configuration tested (IVA – High Swirl) utilized the same surface area, compression ratio and quench area with additional swirl. The third configuration tested (VD – Super High Swirl) utilized an additional approximate 110% increase in swirl together with a 33.9% squish area and a compression ratio of 12.7:1.

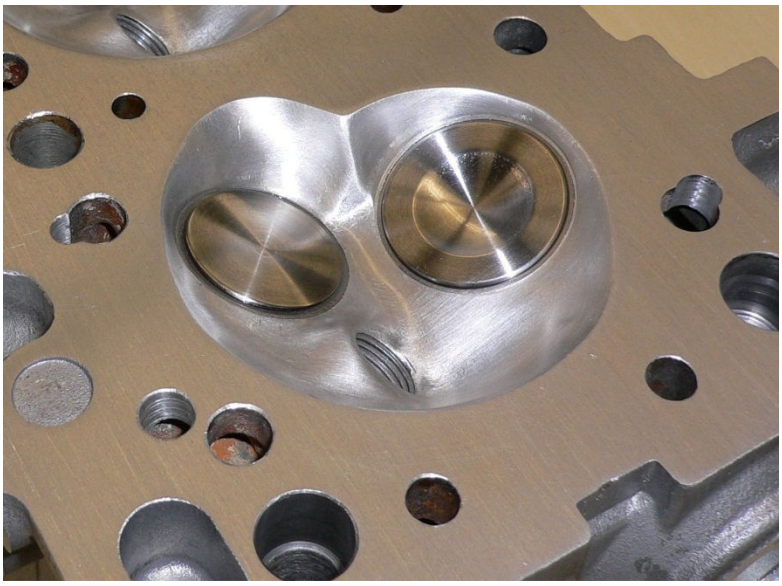

Figure 7– Low Swirl chamber, Swirl Ratio=0.38, Squish Area 18.4% CR 12.2:1

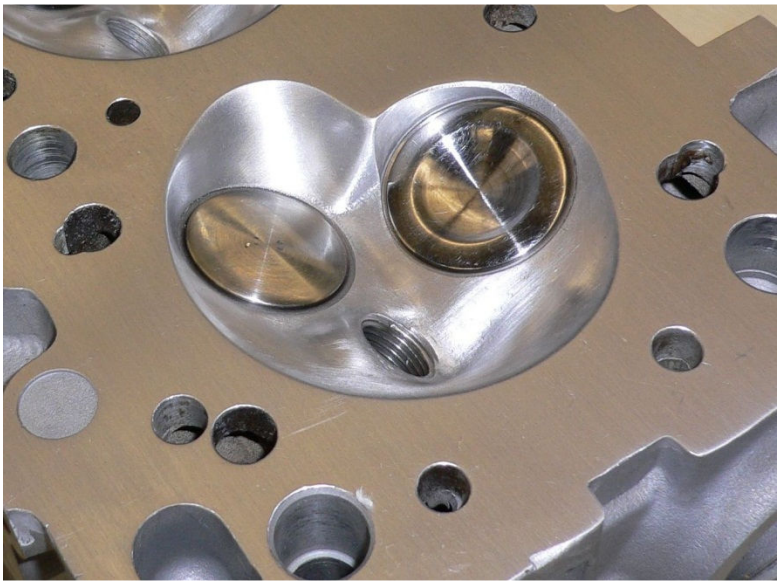

Figure 8– High Swirl chamber, Swirl Ratio=1.50, Squish Area 18.4% CR 12.2:1

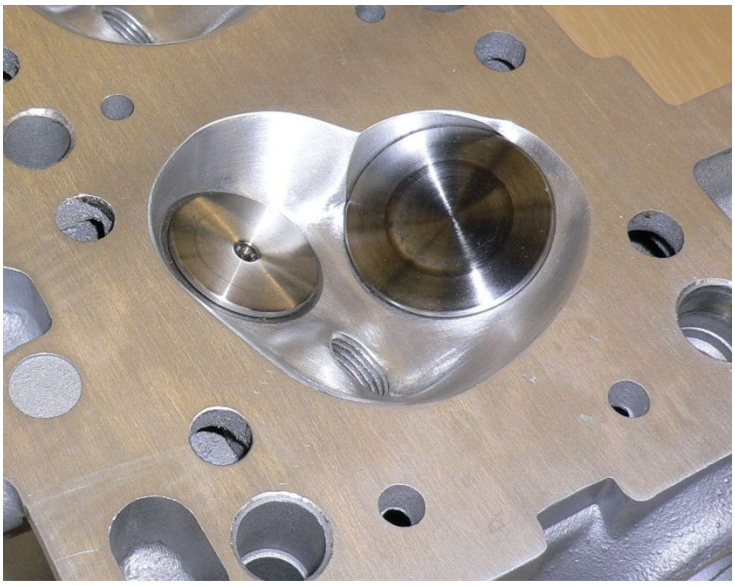

Figure 9 – Super High Swirl chamber, Swirl Ratio=3.20, Squish Area 33.9% CR 12.7:1

The fuel delivery system was composed of a standard minor diameter radial inlet venturi gaseous fuel mixer. To provide the desired cylinder to cylinder fuel distribution, the gas mixture entered a 175 cc pre-chamber before passing through a 6.4 cm^2 orifice into the intake manifold (Figure 10, Figure 11, and Figure 12). This intake geometry produced a 20 mm*Hg intake manifold vacuum at wide open throttle.

Figure 10 - Gas Mixer

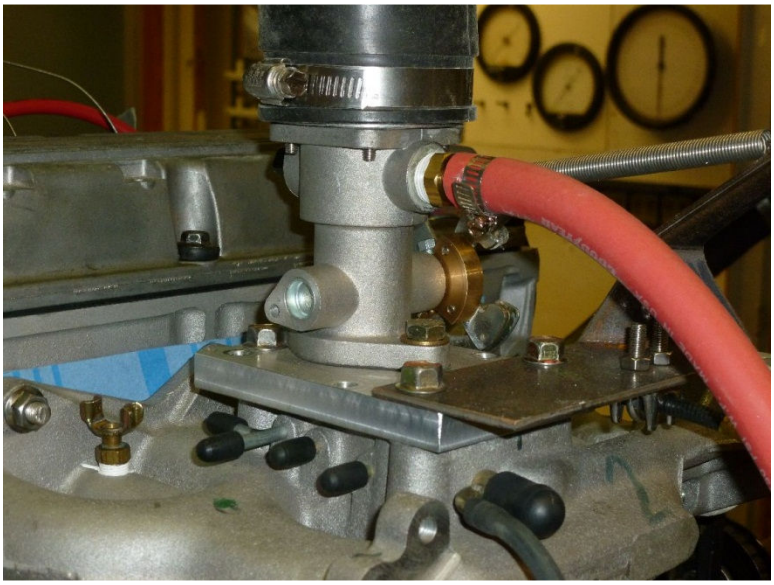

Figure 11 - Gas Mixer, Side View

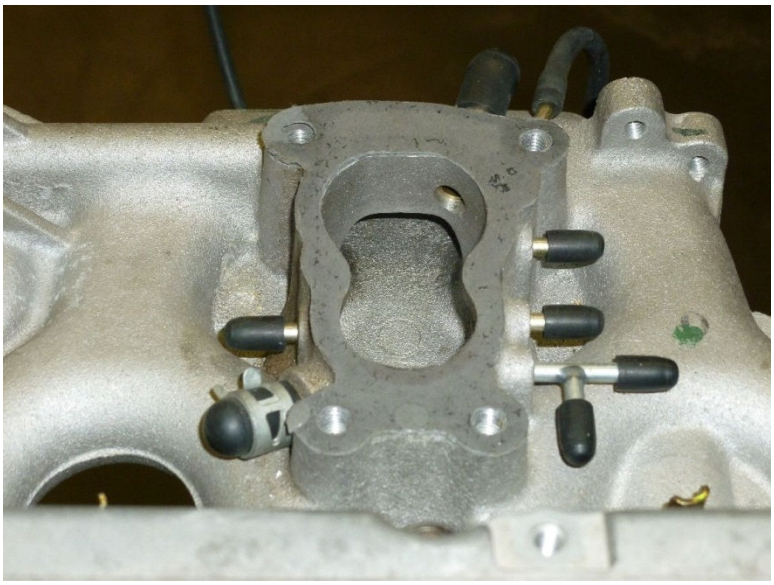

Figure 12 - Intake manifold

Variation in exhaust gas temperature was used as a measure of cylinder to cylinder air fuel ratio distribution. To measure exhaust gas temperature a spacer plate was created to allow thermo couples to be placed in the exhaust flow. The plate and thermo couple can be seen in Figure 13. The average range of temperature differences between cylinders 2, 3, and 4 was plus or minus 2.5°C. The exhaust gas temperature from cylinder 1 was always lower than the other three cylinders and was about 15° C lower at light loads and 35° C lower at high loads. This was due to the exhaust gas recirculation port cast into the number 1 exhaust port. Exhaust gas recirculation was not utilized in the data presented in this paper. The port and adjoining passageway was blocked on the intake side of the cylinder head. This allowed the pulsating flow of exhaust gases from cylinder 1 to enter and exit this water jacket cooled passageway, lowering the exhaust temperature of the gases measured downstream.

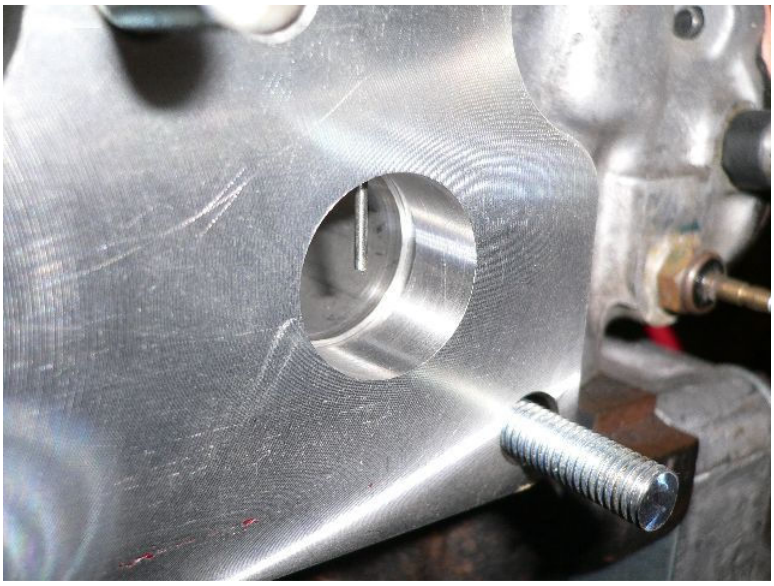

Figure 13 - Thermocouple in Exhaust

The same behavior occurred when operating the engine with port fuel injection seen in Figure 14. The cylinder one exhaust gas temperature was always lower than the other three cylinders by a similar amount. This occurred even when the fuel injector from cylinder one was swapped with an injector from another cylinder.

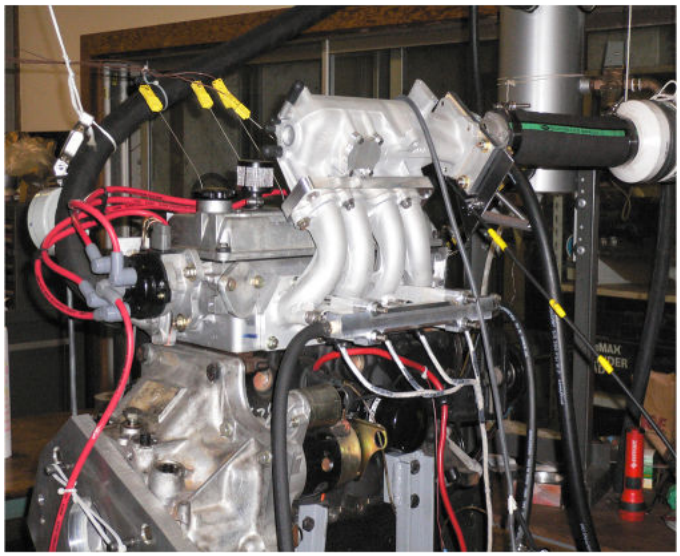

Figure 14 - Engine setup with Port Fuel Injection

Three engine configurations were chosen for testing in this research effort. Each of the configurations was constructed utilizing the same short block and one of the combustion chamber/intake valve combinations listed in Table 2 (Figure 7, Figure 8, and Figure 9). The first four cylinder configurations (IA, IB, IC, and ID) listed in Table 2 were formed by rotating the combustion chamber in three steps a total of 9° at the cylinder head gasket surface. This allowed the swirl intensity to be varied while holding compression ratio, squish percent and surface area constant. Cylinder head IA (Figure 7) had the combustion chamber positioned to create a 65° angle between the gasket surface and the combustion chamber wall near the intake valve. As the combustion chamber was rotated in the respective cylinder heads the combustion chamber wall moved closer to the intake valve. After 9° of rotation (IVA) (Figure 8) the wall was parallel to the valve stem and 1.14 mm from the head of the valve. The rotation of the chamber created increases in swirl, first noted at high valve lifts (IIA and IIIA) and finally at 2.54 mm valve lift (IVA). The airflow capacity was reduced as swirl increased. The radius on the edge between the shrouding combustion chamber wall and the cylinder head gasket surface was critical. A radius of 1.5 mm at the interface of these two surfaces would reduce swirl 25% at 5.08 mm intake valve lift and 60% at 7.62 mm intake valve lift. The only difference in the last three cylinder head configurations in Table 2 (VB, VC, VD) was the intake valve head diameter. The effects of combustion chamber wall to intake valve clearance can be seen in the data of Table 2. Cylinder head configuration VB had a chamber wall to valve clearance of 0.5 mm. Configuration VC had a clearance of 1.22 mm and VD (Figure 9) at a clearance of 2.10 mm. As clearance is increased, swirl is reduced and airflow is increased. This is most apparent at low lifts where the pressure

drop between the wall and valve is similar in magnitude to the pressure drop between the valve seat and valve. The combustion chamber used with the last three cylinder head configurations was smaller in volume producing a 12.7:1 compression ratio. The smaller chamber had an additional squish area added on the spark plug side of the combustion chamber resulting in a 33.9% squish area. With the exception of the pistons, pins and rings all of the engine components were standard parts manufactured for production engines.

It is desirable to control spark advance electronically. It was controlled using a Haltech computer and cam position sensor. The standard distributor did not have a cam position sensor and could not be easily modified to allow cam position sensing. The Mazda B-series shop manuals revealed that the 1.6L Mazda SOHC 4 valve California engine used from 1993-1995 could be used as a substitute cam position sensor. Though it was not possible to locate a California car, the Hollander Interchange Manuals showed the same distributor was used in the 1992-1993 MX3. This distributor was used for all testing to facilitate control of the spark advance. The distributor is shown in Figure 15.

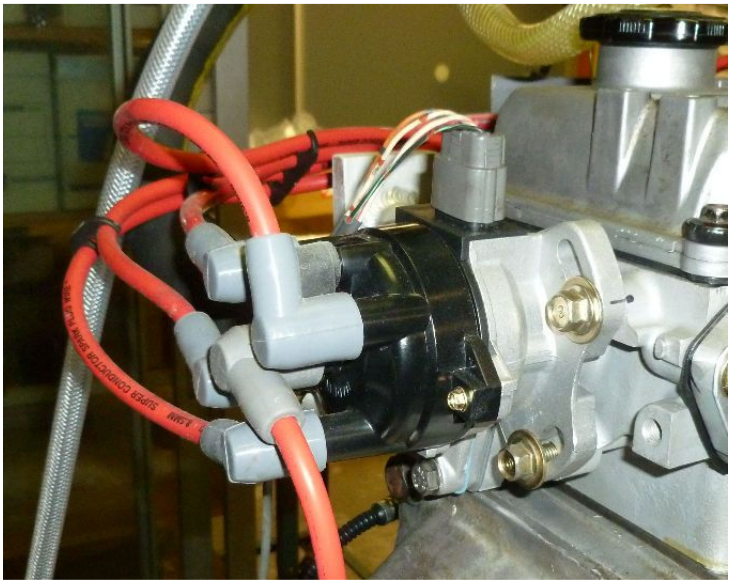

Figure 15 - Distributor with Cam Position Sensor

The first engine configuration tested utilized combustion chamber/intake valve combination IA (Table 2). The Low Swirl engine configuration represented the baseline engine configuration and incorporated the minimum squish and swirl tested. As a result, best efficiency equivalence ratio fell between λ=1.23 and λ=1.31. Maximum brake thermal efficiency (BTE) was 37.2% occurring at 780 kPa BMEP, λ=1.29. Maximum load was 875 kPa BMEP, with a BTE of 36.8% and λ=1.23. Higher BMEP would have been possible with richer mixtures but BTE began to drop noticeably. Figure 16 shows BTE versus torque. 114.2 N*m. of torque (875 kPa BMEP) was reached with minimum enrichment from best efficiency air-fuel equivalence ratio. Figure 16 also shows the BTE shows the BTE verses torque for the original engine if rebuilt using the standard parts designed for gasoline operation.

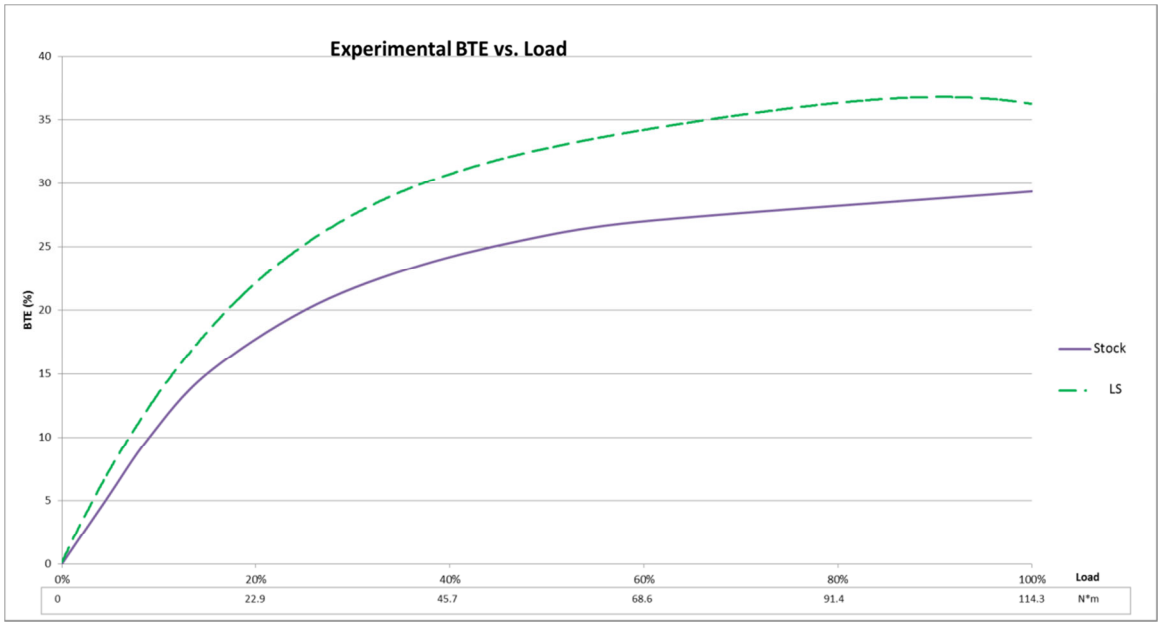

Figure 16- BTE vs. Load for Low Swirl Engine

The second engine configuration tested utilized combustion chamber/intake valve combination IV A (Table 2) (Figure 8). This High Swirl configuration was identical to the first engine configuration except the combustion chamber was, as previously mentioned, rotated 9°. This produced a large increase in average swirl ratio from 0.38 to 1.50 by allowing the combustion chamber wall next to the intake valve to shroud the passage of air past that side of the valve. Clearance between the edge of the intake valve and the shrouding wall of the combustion chamber was 1.14 mm.

The best BTE for the High Swirl engine configuration fell between λ=1.40 and λ=1.49 fuel air equivalence ratio. Maximum BTE for the High Swirl configuration was 35.9% occurring at 729 kPa BMEP, λ=1.40. Maximum load was 875 kPa BMEP, with a BTE of 33.4% because a fuel air equivalence ratio of λ=1.09 was required to reach this power output. Figure 17 shows the BTE versus torque for both the Low Swirl and the High Swirl engine.

It can be seen that between 260 kPa and 570 kPa BMEP output the Low Swirl and High Swirl engine configurations delivered nearly identical BTE values. This occurred with the High Swirl engine employing leaner fuel air ratios. The High Swirl engine configuration demonstrated improvements in BTE as high as 12% at loads below 260 kPa. While at loads above 725 kPa required fuel air mixtures richer than λ=1.40, the BTE dropped rapidly for loads higher than 725 kPa. A literature review of similar lean burn combustion engines shows several other engines with similar mixtures. This is expected as the swirl ratio and squish area percentage of the High Swirl engine was still similar to production automobile engines and the research from the literature was conducted with mildly modified automobile engines. Previous lean limits of combustion

for LPG were determined to be λ=1.47 (Quader, 1974). Another experiment showed combustion of LPG as lean as λ=1.48 at a compression ratio of 11.4:1 and λ=1.42 at a compression ratio of 10.2:1(Li, 2002). Both of these papers show a relatively similar lean limit. Thring demonstrated lean combustion in a gasoline engine with a compression ratio of 11:1 and BMEP 2.5bar with a swirl ratio of .25 and λ=1.28 (Thring, 1982). Were either the Low Swirl or High Swirl engine to be utilized to power a 17 kW genset with extended high load operation, the Low Swirl engine configuration would be the best choice. If the desire were to power a 15 kW genset (maximum BMEP 743 kPa) the High Swirl configuration would be preferable. This would be particularly true if an output below 5 kW was expected for long intervals.

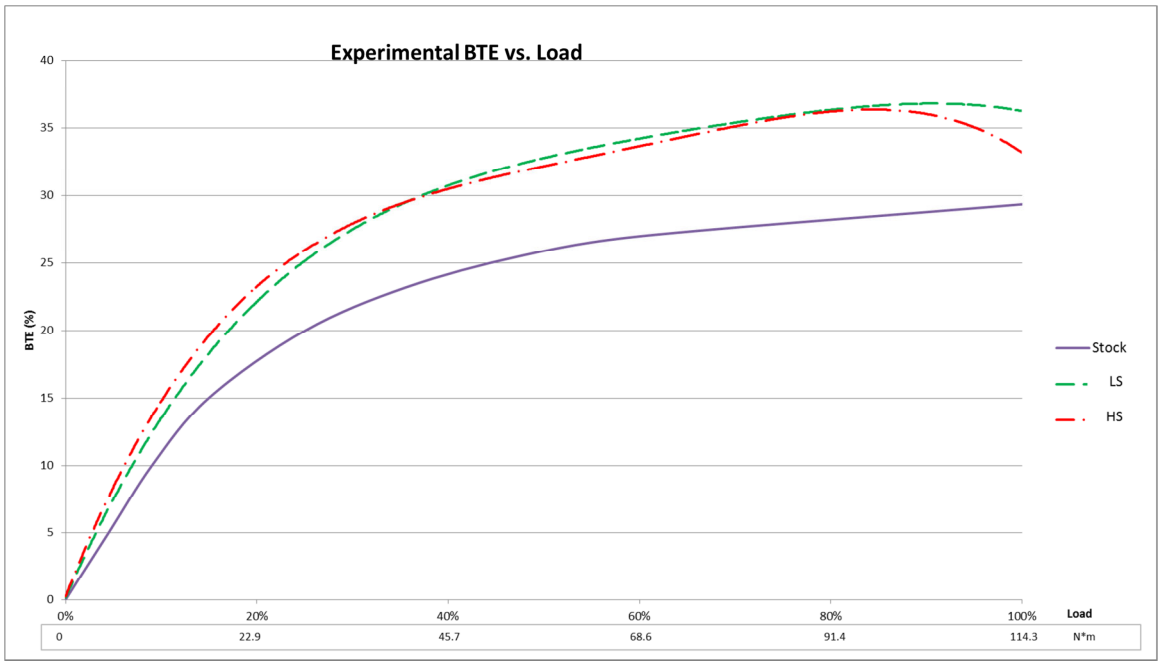

Figure 17 - BTE vs. Load for Low Swirl and High Swirl Engines

The third engine configuration tested (Super High Swirl) utilized combustion chamber and intake valve configuration VD. This configuration required a larger intake valve to increase the average swirl ratio to 3.20. Additionally the compression ratio was

increased to 12.7:1 by reducing the combustion chamber volume with the addition of more squish area. The new squish area was 33.9%. The cylinder head employed a low duration cam profile which allowed the intake valve to close 6° early increasing volumetric efficiency while reducing residual back flow into the intake manifold by approximately 50%. This cam shaft operated with low force valve springs. The valve seat force was reduced from 187 N to 107 N, and the maximum valve lift force was reduced from 512 N to 254 N. Tests with and without the new valve springs showed a 3450 Pa to 5170 Pa reduction in fmep, this is due to lower spring forces. Titanium retainers shown in Figure 20 were also tested and produced no discernible change in fmep. The third engine also employed “rhino” feet type valve adjusters on modified rocker arms. “Rhino” feet type adjusters are articulated adjusters. They were utilized because valve adjuster replacement is necessary at the time of engine rebuild and the “rhino” feet type adjusters are more reliable than the original adjusters. These were installed by employing a redesign of the hydraulic rocker arms from the 1.6L SOHC two valve engine. Figure 18 and Figure 19 show both style rocker arms.

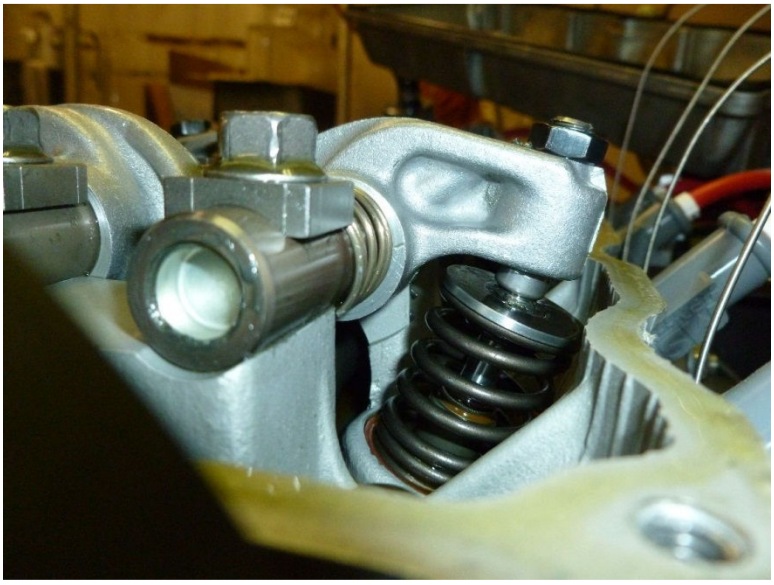

Figure 18 - “Rhino” feet rocker arms, Super High Swirl Engine

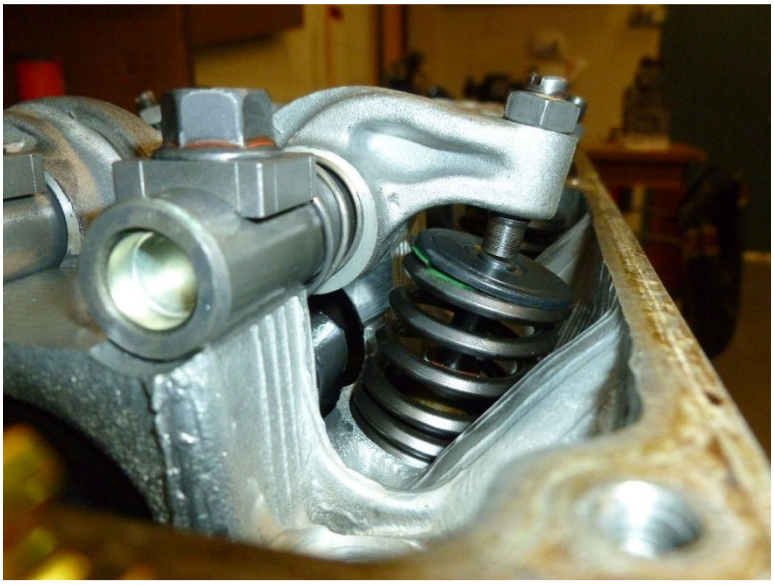

Figure 19 - Stock rocker arms, Low Swirl and High Swirl Engine

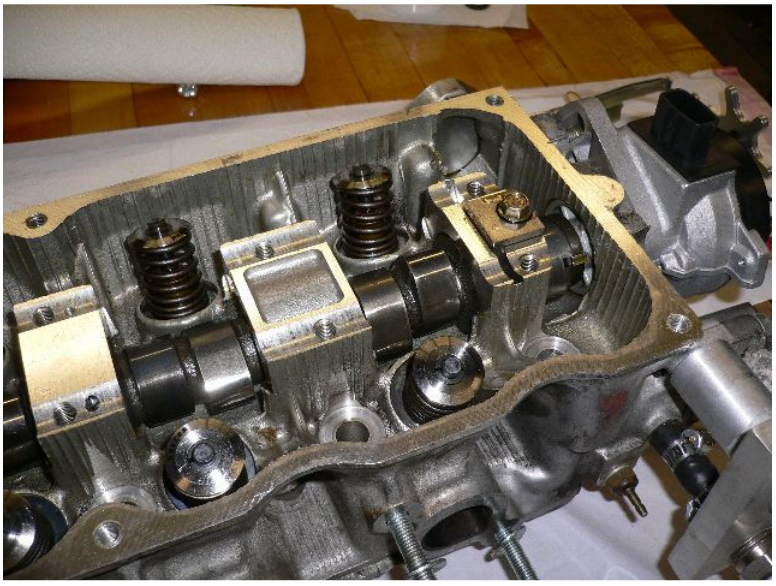

Figure 20 - Titanium Valve Retainers

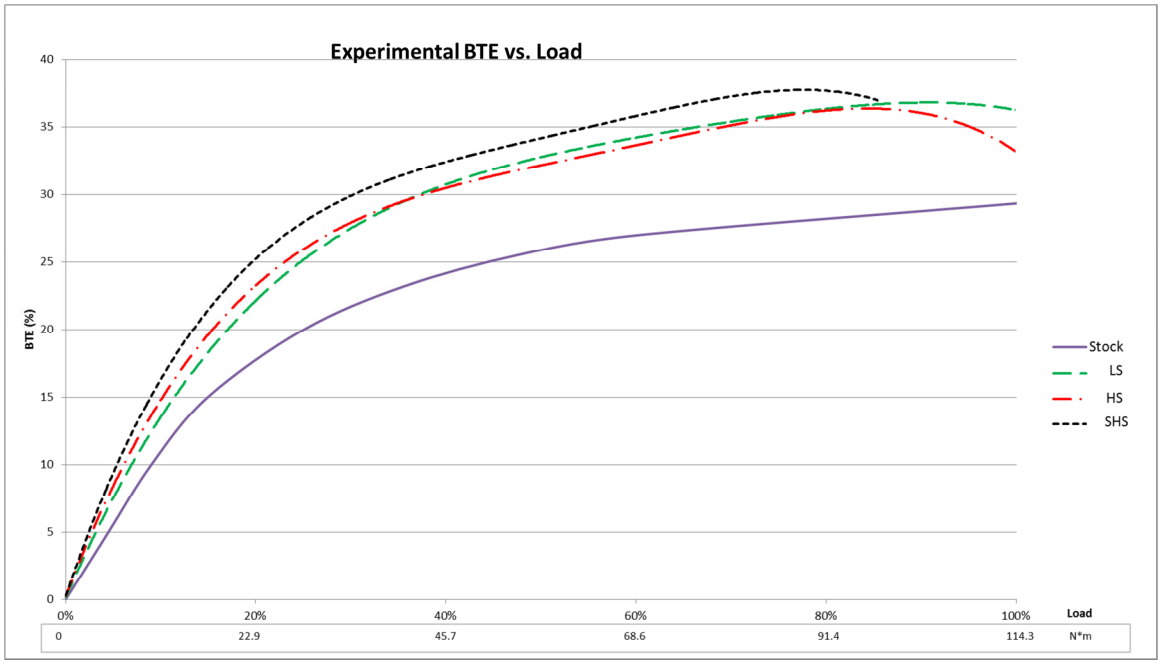

Figure 21 - BTE vs. Load for Low Swirl, High Swirl and Super High Swirl Engines

The Super High Swirl engine developed a maximum BTE of 37.5% with λ in the range of 1.63 to 1.66 at a BMEP of 876 kPA. This experiment shows that the lean limit of combustion for propane can be extended to mixtures leaner than λ=1.5. Due to the high gas velocities running richer mixtures anywhere near stoichiometric becomes impractical with this engine design.

The Super High Swirl engine configuration can be compared against similar engines. Experimentation using a much larger 4.0L six cylinder engine on LPG and was able to attain a BTE of 37.18% at λ=1.4 with a compression ratio of 11.7:1 at 1800RPM (Baker et al., 2005). Experimentation on a 2.0L LPG engine and was able to obtain a maximum BTE of 35% with a compression ratio of 10.0:1, 36.2% BTE at 12.0:1 and 37.2% BTE at 13.0:1 (Mizushima et al., 2009). Both of these research efforts utilized much larger cylinder volumes, resulting in lower surface to volume ratios. The lower surface to volume ratios should allow a higher BTE than the 1.6L engine of this study. They

employed sophisticated fuel injection delivery systems. These type of fuel delivery systems would be more expensive than the venture mixer/prechamber approach utilized in this research effort.

Chapter 3 Model

Combustion:

The combustion model used is based on the model developed by Ferguson for the arbitrary heat release of fuel inducted engines (Ferguson,C. 1986, pg. 168-174). The following equations for combustion unless otherwise noted are from Ferguson. The control volume considered for combustion is modeled by equation 2. The properties of the fluid in the combustion chamber are determined using the subroutines FARG and ECP. These subroutines use state variables of temperature and pressure to determine the properties of the fluid. The energy within the system is split into two sets of constituents, burned and unburned. Both are assumed to have the same pressure but temperature is not necessarily the same. The burn rate is modeled using the Wiebe function.

$$\mathbf{m}\frac{\mathbf{du}}{\mathbf{d\theta}} + \mathbf{u}\frac{\mathbf{dm}}{\mathbf{d\theta}} = \frac{\mathbf{dQ}}{\mathbf{d\theta}} - \mathbf{P}\frac{\mathbf{dV}}{\mathbf{d\theta}} - \frac{\dot{\mathbf{m}}_{\mathbf{l}}\mathbf{h}_{\mathbf{l}}}{\boldsymbol{\omega}} \quad \text{Equation 2}$$

The energy contained in the system is determined by the sum of the energies of the burned and unburned constituents. The energy of the system is shown in equation 3. The burned and unburned energies are ($u_b \; and \; u_u$). The energy of the burned and unburned fluids is based on their shared pressure and respective temperatures.

$$u = xu_b + (1 - x)u_u \quad \text{Equation 3}$$

The specific volume of the fluids is based on an equation of the same form as the energies. The equation for specific volumes is seen in equation 3.

$$\boldsymbol{v = xv_b + (1 - x)v_u} \quad \text{Equation 4}$$

Specific volume and energy is considered to only be only a function of temperature and pressure. Differentiating with respect to crank angle and substituting the natural logs gives the following equations.

$$\frac{dv_b}{d\theta} = \frac{v_b}{T_b}\frac{\partial \ln v_b}{\partial \ln T_b}\frac{dT_b}{d\theta} + \frac{v_b}{P}\frac{\partial \ln v_b}{\partial \ln P}\frac{dP}{d\theta} \quad \text{Equation 5}$$

$$\frac{dv_u}{d\theta} = \frac{v_u}{T_u}\frac{\partial \ln v_u}{\partial \ln T_u}\frac{dT_u}{d\theta} + \frac{v_u}{P}\frac{\partial \ln v_u}{\partial \ln P}\frac{dP}{d\theta} \quad \text{Equation 6}$$

$$\frac{du_b}{d\theta} = \left(c_{Pb} - \frac{Pv_b}{T_b}\frac{\partial \ln v_b}{\partial \ln T_b}\right)\frac{dT_b}{d\theta} - v_b\left(\frac{\partial \ln v_b}{\partial \ln T_b} + \frac{\partial \ln v_b}{\partial \ln P}\right)\frac{dP}{d\theta} \quad \text{Equation 7}$$

$$\frac{du_u}{d\theta} = \left(c_{Pu} - \frac{Pv_u}{T_u}\frac{\partial \ln v_u}{\partial \ln T_u}\right)\frac{dT_u}{d\theta} - v_u\left(\frac{\partial \ln v_u}{\partial \ln T_u} + \frac{\partial \ln v_u}{\partial \ln P}\right)\frac{dP}{d\theta} \quad \text{Equation 8}$$

When equations 3, 7 and 8 are substituted into equation 2, the new equation is of the form seen in equation 9.

$$mx\left(c_{Pb} - \frac{Pv_b}{T_b}\frac{\partial \ln v_b}{\partial \ln T_b}\right)\frac{dT_b}{d\theta} + m(1-x)\left(c_{Pu} - \frac{Pv_u}{T_u}\frac{\partial \ln v_u}{\partial \ln T_u}\right)\frac{dT_u}{d\theta} -$$

$$\frac{dP}{d\theta}\left[mxv_b\left(\frac{\partial \ln v_b}{\partial \ln T_b} + \frac{\partial \ln v_b}{\partial \ln P}\right) + mv_u(1-x)\left(\frac{\partial \ln v_u}{\partial \ln T_u} + \frac{\partial \ln v_u}{\partial \ln P}\right)\right] + m\frac{dx}{d\theta}(u_b - u_u) + u\frac{dm}{d\theta} =$$

$$\frac{dQ}{d\theta} - P\frac{dV}{d\theta} - \frac{\dot{m}_l h_l}{\omega} \quad \text{Equation 9}$$

The Wiebe function (Ferguson, pg 80 and Heywood pg 768) determines heat addition to the control volume during combustion. The Wiebe function is shown in equations 10 and 11. The coefficients b and n in equation 10 determine the rate of burn over the burn period. Heywood used b=5 and n=3 based on experimental results. The coefficients can be fitted to experimental data from the given engine if data is available. A comparison of the two can be seen in Figure 22. It can be seen that the second equation has a slower initial burn rate and approaches complete burn faster than equation one over the second half of the burn duration.

$$x = 1 - e^{-b\left[\left(\frac{\theta-\theta_s}{\theta_b}\right)^n\right]} \quad \text{Equation 10}$$

$$x = \frac{1}{2}\left(1 - \cos\left(\frac{\pi(\theta - \theta_s)}{\theta_b}\right)\right)$$ Equation 11

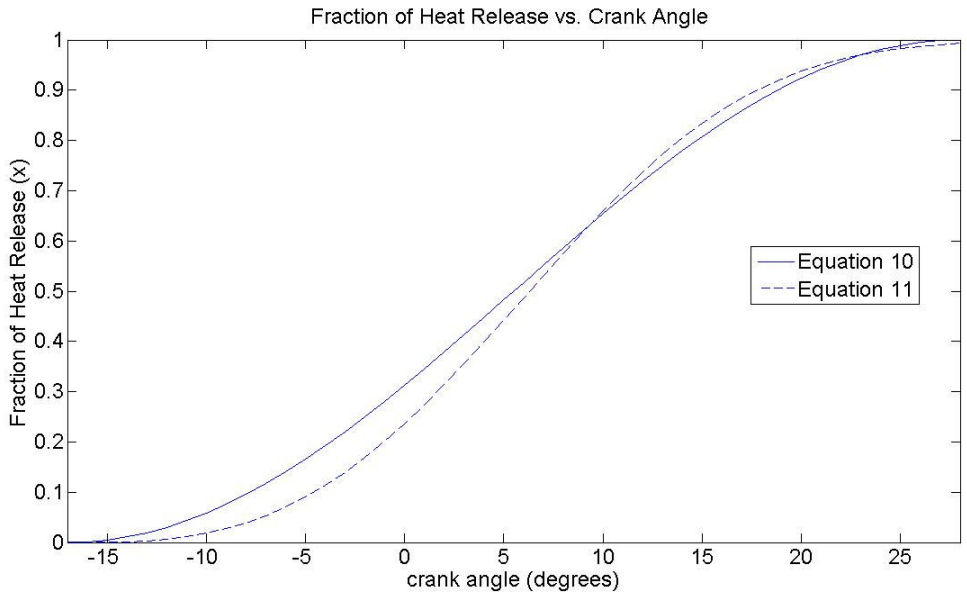

Figure 22- Comparison of Equations 10 and 11

In order to determine the mass lost during combustion across the piston rings a general equation is developed. Mass loss is only considered to be a function of engine speed. To correlate the mass loss with experimental findings the constant C is introduced.

$$\frac{dm}{d\theta} = -\frac{C\,m}{\omega}$$ Equation 12

$$m = m_1 e^{-\frac{C(\theta - \theta_1)}{\omega}}$$ Equation 13

The heat loss is the sum of the heat flow out of the burned and unburned fluids. The only form of heat transfer considered is convection. The heat transfer coefficients are determined by the Woschni model and will be described in depth later.

$$\frac{dQ}{d\theta} = -\frac{(\dot{Q}_b + \dot{Q}_u)}{\omega}$$ Equation 14

$$\dot{Q}_b = hA_b(T_b - T_w)$$ Equation 15

$$\dot{Q}_u = hA_u(T_u - T_w)$$ Equation 16

$$A_b = \left(\frac{\pi b^2}{2} + 4\frac{V}{b}\right)\sqrt{x}$$ Equation 17

$$A_u = \left(\frac{\pi b^2}{2} + 4\frac{V}{b}\right)\left(1 - \sqrt{x}\right)$$ Equation 18

$$V = V_{tdc}\left(1 + \frac{CR-1}{2}\left\{1 - \cos\theta + \frac{1}{\epsilon}\langle 1 - \sqrt{1 - \epsilon^2 \sin^2\theta}\rangle\right\}\right)$$ Equation 19

The equation for the specific volume of the system is found by differentiating equation 4 and substituting 5, 6 and 12 into it.

$$\frac{1}{m}\frac{dV}{d\theta} - \frac{V}{m^2}\frac{dm}{d\theta} = x\frac{dv_b}{d\theta} + (1-x)\frac{dv_u}{d\theta} + (v_b - v_u)\frac{1}{m}\frac{dx}{d\theta}\frac{dV}{d\theta} + \frac{VC}{m\omega} = x\frac{v_b}{T_b}\frac{\partial \ln v_b}{\partial \ln T_b}\frac{dT_b}{d\theta} +$$

$$(1-x)\frac{v_u}{T_u}\frac{\partial \ln v_u}{\partial \ln T_u}\frac{dT_u}{d\theta} + \left(x\frac{v_b}{P}\frac{\partial \ln v_b}{\partial \ln P}\frac{dP}{d\theta} + (1-x)\frac{v_u}{P}\frac{\partial \ln v_u}{\partial \ln P}\frac{dP}{d\theta}\right)\frac{dP}{d\theta} + (v_b - v_u)\frac{dx}{d\theta}$$

Equation 20

The unburned fluid entropy leaving the system is seen in equation 21. The derivate of entropy with respect to crank angle is seen in equation 22. When combined with equation 16 they form equation 23.

$$\dot{Q}_u = -\omega m(1-x)T_u\frac{\partial s_u}{\partial \theta}$$ Equation 21

$$\frac{\partial s_u}{\partial \theta} = \left(\frac{c_{Pu}}{T_u}\right)\frac{dT_u}{d\theta} - \frac{v_u}{T_u}\frac{\partial \ln v_u}{\partial \ln P}\frac{dP}{d\theta}$$ Equation 22

$$c_{Pu}\frac{dT_u}{d\theta} - v_u\frac{\partial \ln v_u}{\partial \ln P}\frac{dP}{d\theta} = \frac{-h\left(\frac{\pi b^2}{2} + 4\frac{V}{b}\right)}{\omega m}\frac{1-\sqrt{x}}{1-x}(T_u - T_w)$$ Equation 23

Ferguson solved the system of equations. The coefficients A, B, C, D and E are used to simplify the equation layout. Equations 29 through 34 use the coefficients to determine the change in pressure, temperature, work, heat transfer, and heat loss at each position crankshaft position.

$$A = \frac{1}{m}\left(\frac{dV}{d\theta} + \frac{VC}{\omega}\right)$$ Equation 24

$$B = h\frac{\left(\frac{\pi b^2}{2} + 4\frac{V}{b}\right)}{\omega m}\left[\frac{dv_b}{c_{Pu}}\frac{\partial \ln v_b}{\partial \ln T_b}\sqrt{x}\frac{(T_b - T_w)}{T_b} + \frac{v_u}{c_{Pu}}\frac{\partial \ln v_u}{\partial \ln T_u}1 - \sqrt{x}\frac{(T_u - T_w)}{T_u}\right]$$ Equation 25

$$C = -(v_b - v_u)\frac{dx}{d\theta} - v_b\frac{\partial \ln v_b}{\partial \ln T_b}\frac{h_u - h_b}{c_{Pb}T_b}\left[\frac{dx}{d\theta} - \frac{(x - x^2)C}{\omega}\right]$$ Equation 26

$$D = x\left[\frac{{v_b}^2}{c_{Pb}T_b}\left(\frac{\partial \ln v_b}{\partial \ln T_b}\right)^2 + \frac{v_b}{P}\frac{\partial \ln v_b}{\partial \ln P}\right]$$ Equation 27

$$E = (1-x)\left[\frac{{v_u}^2}{c_{Pu}T_u}\left(\frac{\partial \ln v_u}{\partial \ln T_u}\right)^2 + \frac{v_u}{P}\frac{\partial \ln v_u}{\partial \ln P}\right]$$ Equation 28

$$\frac{dP}{d\theta} = \frac{A+B+C}{D+E}$$ Equation 29

$$\frac{dT_b}{d\theta} = \frac{v_b}{c_{Pb}}\frac{\partial \ln v_b}{\partial \ln T_b}\frac{A+B+C}{D+E} - h\frac{\left(\frac{\pi b^2}{2}+4\frac{V}{b}\right)}{\omega m c_{Pb}}(T_b - T_w)\frac{\sqrt{x}}{x} + \frac{(h_u - h_b)}{x c_{Pb}}\left(\frac{dx}{d\theta} + (x^2 - x)\frac{C}{\omega}\right)$$ Equation 30

$$\frac{dT_u}{d\theta} = \frac{v_u}{c_{Pu}}\frac{\partial \ln v_u}{\partial \ln T_u}\frac{A+B+C}{D+E} - h\frac{\left(\frac{\pi b^2}{2}+4\frac{V}{b}\right)}{\omega m c_{Pu}}(T_u - T_w)\frac{\left(1-\sqrt{x}\right)}{(1-x)}$$ Equation 31

$$\frac{dW}{d\theta} = P\frac{dP}{d\theta}$$ Equation 32

$$\frac{dQ_l}{d\theta} = \frac{h}{\omega}\left(\frac{\pi b^2}{2} + 4\frac{V}{b}\right)\left[\sqrt{x}(T_b - T_u) + \left(1-\sqrt{x}\right)(T_u - T_w)\right]$$ Equation 33

$$\frac{dH_l}{d\theta} = \frac{Cm}{\omega}[h_u(1-x^2) - h_b x^2]$$ Equation 34

Heat Transfer:

Woschni developed a model for determining the convective heat transfer based on piston motion and combustion (Woschni, 1967). Radiation and conductive heat transfer were not considered, since they represent only a small percentage of total heat transfer inside the combustion chamber. The heat transfer model determined by Woschni can be seen in the following equation (Woschni, 1967).

$$h = 110\ b^{-0.2}p^{0.8}T^{-0.53}\left[C_1 c_m + C_2\frac{V_s T_1}{p_1 V_1}(p - p_0)\right]^{0.8}\left(\frac{kcal}{m^2}°C\right)$$ Equation 35

The terms $p_1$and $T_1$are reference parameters at a known volume (V_1). The term V_s is the swept volume. The motoring pressure is p_0 and mean piston speed c_m. Woschni determined the constants to be $C_1 = 2.28$ and $C_2 = 3.24 * 10^{-3} m/s°C$.

To take into account the velocity of fluids in the combustion chamber, the Woschni model was modified to include parameters for swirl (V_{SW}) and squish (V_{SQ}) velocities. This modification from the original model allowed for the changes in heat transfer by the additional gas velocities. Swirl was considered during the intake and compression phases. Squish was only considered during combustion before TDC. To take into account the additional velocities associated with squish, swirl and piston speed (V_p) the root mean square of the velocities was combined to replace the mean piston speed term (c_m). Woschi's equation was modified to the following form. In the modified Woschni equation (c_m) was replaced with (V_g).

$$h = 110\ b^{-0.2} p^{0.8} T^{-0.53} \left[C_1 V_g + C_2 \frac{V_s T_1}{p_1 V_1}(p - p_0)\right]^{0.8} \left(\frac{kcal}{m^2}°C\right) \quad \text{Equation 36}$$

$$V_g = \sqrt{{V_{SQ}}^2 + {V_{SW}}^2 + {V_p}^2} \quad \text{Equation 37}$$

$$V_{SQ} = \frac{b\ SQ\%\ V_p}{4\sqrt{1 - SQ\%}\ X_1} \quad \text{Equation 38}$$

The squish velocity was determined from the volume of gas forced up by the piston into the squish area. Since the gasses in the combustion chamber were all considered to be the same pressure, this same volume of gas would need to be forced out of the squish area into the rest of the chamber. The area of the gasses forced out was determined from the distance between the piston and the top of the combustion chamber (X_1) and the diameter of the non-squished area.

The model determined the heat loss for burned and unburned fluids as seen in the following equations 39 and 40. These equations are found when combing equations 17 and 19 into 15 and 16.

$$\boldsymbol{Q_u = h_u \left(\frac{\pi b^2}{2} + \frac{4V}{b}\right)\left(1 - \sqrt{x}\right)(T_u - T_w)}$$ Equation 39

$$Q_b = h_b \left(\frac{\pi b^2}{2} + \frac{4V}{b}\right)\sqrt{x}(T_b - T_w)$$ Equation 40

The heat losses after exhaust gasses leave the combustion chamber were captured using a correlation to the Nusselt number similar to Meisner & Sorenson where the Nusselt number is a function of Reynolds. The Meisner equation was modified to take into account the curved exhaust port used in experimentation. The equation for the value of the Nusselt number used in the exhaust port can be seen in the following equation. The value of the coefficent (C_{exh}) is a weighting coeffient used to match the heat losses.

$$Nu = C_{exh} Re^{.769}$$ Equation 41

The exit temperature was determined considering only convective heat transfer between the exhaust gasses and the exhaust port surfaces. The temperature of the bulk exhaust gasses exiting the exhaust port (T_{b2}) were found by solving the following equations. Where h is the heat transfer coefficient, d is the diameter of the exhaust port, L is the length of the exhaust port, $T_w$is the surface temperature of the exhaust port and $T_{b1}$is the bulk temperature of gasses entering the exhaust port from the combustion chamber.

$$h\pi d\ L\left(T_w - \frac{T_{b1} - T_{b2}}{2}\right) = \dot{m} c_p (T_{b2} - T_{b1})$$ Equation 42

$$h = \frac{k\ Nu}{d}$$ Equation 43

Frictional Model:

The model for friction utilized here was chosen from two published frictional models. The model developed by Patton, Nitschke and Heywood used scaling laws and experimental results to model friction for a variety of frictional losses. They found their model to give reliable results. Later their equations were revisited and revised by

Sandoval and Heywood. The later model was used for theoretical results. A similar model was developed by Bishop. The results of both sets of modeling were compared.

The model described here was developed by Sandoval and Heywood (Sandoval, 2003). The equation for frictional losses at the crank is seen here in equation 44. The previous model did not have the viscosity terms in the frictional equations. Instead they were included in the experimental coefficients. Equations 45 and 46 model the reciprocating frictional losses both with and without pressure loading. Equation 47 models the losses seen in the valve train mechanical components. The coefficients of the valve train components are given in Table 3. The modeling of the auxiliary losses is given in equation 48 and is dependent on engine speed. The equations for pumping losses are seen in equations 49 and 50.

$$fmep_{crank} = 1.22e^{5}\left(\frac{D_b}{B^2 S\, n_c}\right) + 3.03e^{4}\sqrt{\frac{\mu}{\mu_0}}\left(\frac{N{D_b}^3 L_b n_b}{B^2 S\, n_c}\right) + 1.35e^{-10}\left(\frac{N^2 {D_b}^2 n_b}{n_c}\right)$$

Equation 44

$$fmep_{recip^{w}/_{o}press} = 2.94e^{2}\sqrt{\frac{\mu}{\mu_0}}\left(\frac{S_p}{B}\right) + 4.06e^{4}\left(\frac{F_t}{F_{t0}}\right)\left(1+\frac{500}{N}\right)\left(\frac{1}{B^2}\right) +$$

$$3.03e^{4}\sqrt{\frac{\mu}{\mu_0}}\left(\frac{N{D_b}^3 L_b n_b}{B^2 S\, n_c}\right)$$

Equation 45

$$fmep_{recip\ w\ press} = 6.89\frac{p_i}{p_a}\left[\sqrt{\frac{\mu}{\mu_0}} + 0.182\frac{F_t}{F_{to}} r_c^{(1.33-KS_p)}\right]$$

Equation 46

$$fmep_{valve\ train} = 244\sqrt{\frac{\mu}{\mu_0}}\left(\frac{N n_b}{B^2 S\, n_c}\right) + c_{ff}\left(1+\frac{500}{N}\right)\frac{n_v}{S\, n_c} + c_{rf}\frac{N n_v}{S\, n_c} +$$

$$c_{oh}\sqrt{\frac{\mu}{\mu_0}}\left(\frac{{L_v}^{1.5}\sqrt{N}\, n_v}{B\, S\, n_c}\right) + c_{om}\left(1+\frac{500}{N}\right)\frac{L_v\, n_v}{S\, n_c}$$

Equation 47

$$fmep_{aux} = 8.3155 + 1.86e^{-3}N + 7.45e^{-7}N^2$$

Equation 48

$$fmep_{intake} = (p_a - p_i) + 3.0e^{-3}\left(\frac{p_i}{p_a}\right)^2\left(\frac{{S_p}^2}{{n_v}^2{r_i}^4}\right) \quad \text{Equation 49}$$

$$fmep_{exhaust} = 0.178\left(\frac{p_i}{p_a}S_p\right)^2 + 3.0e^{-3}\left(\frac{p_i}{p_a}\right)^2\left(\frac{{S_p}^2}{{n_v}^2{r_e}^4}\right) \quad \text{Equation 50}$$

Sandoval's model is applicable for many different valve train configurations. The coefficients for different configurations can be seen in the following table.

Table 3 - Coefficient for Valve train friction (Sandoval, 2003)

TYPE	c_{ff}	c_{rf}	c_{oh}	c_{om}
SOHC (finger follower)	600	0.0227	0.2	42.8
SOHC (rocker follower)	400	0.0151	0.5	21.4
SOHC (direct acting)	200	0.0076	0.5	10.7
DOHC (finger follower)	600	0.0227	0.2	25.8
DOHC (direct acting)	133	0.0050	0.5	10.7
OHV	400	0	0.5	32.1

Table 4 - Friction Coefficients (Sandoval, 2003)

Coefficient	Value
K	$2.38e^{-2}$

Bishop's equations followed a similar form. Bishop defined the following frictional loss equations (Bishop, 1964). The equations for crankcase frictional losses were defined into several area pumps, valve gear, and bearings.

$$fmep_{pumps} = 0.39\left(\frac{N}{1000}\right)^{1.5} \quad \text{Equation 51}$$

$$fmep_{valve\ gear} = \left(30 - \frac{4N}{1000}\right)\frac{GH^{1.75}}{B^2S} \quad \text{Equation 52}$$

$$fmep_{bearings} = \frac{KBN}{S}\frac{1}{1000} \quad \text{Equation 53}$$

$$K = \frac{6.0\left(a^2c+\frac{b^2d}{m}+e^2f\right)}{B^3}$$ Equation 54

The variables in Bishops equation for K (Equation 54) is a coefficient based on the geometry of the bearing surfaces. The units are all in inches and are a=Main bearing diameter, b=Rod bearing diameter, c=length of main bearings/ cylinder, d=Rod bearing length, e=Accessory bearing diameter, f=Length of accessory bearing, m=number of pistons/ rod bearing, and n=overall number of rings per cylinder. These variables are unique to the bishop frictional equations. Bishop developed the following equation for the pumping losses.

$$fmep_{pumping} = \sqrt{\frac{IMEP_c}{1.63}}\left(1.30\left(\frac{N}{1000}\right)^{1.70}\left(\frac{0.0758}{F}\right)^{1.28}\right)$$ Equation 55

$$F = \frac{12.7\ H^2\ C}{D}\sqrt{162 + R_c^2}$$ Equation 56

$$P_e = 0.0312\ P'_e\left(\frac{IMEP_c\ N}{100000}\right)^2$$ Equation 57

$$fmep_{throttle} = \frac{P_e}{2.75} + P_1$$ Equation 58

$$fmep_{Blowby} = \sqrt{\frac{(p_a-p_1)}{14.2}}\left[1.72{R_c}^{0.4} - \left(\frac{N}{1000}\right)^{1.185}(0.49 + 0.015R_c)\right]$$ Equation 59

Bishop used the following variables to determine the pumping losses. All the variables were in units of inches where C=Number of cylinders, D=Engine Displacement, F=Valve to combustion chamber area, and H=Intake valve head diameter. He defined the following equations for friction at the piston.

$$fmep_{piston\ viscous} = \frac{21.93\ (MV_p)}{(B\ S)\ 1000}$$ Equation 60

$$fmep_{static\ ring} = \frac{2.11\ S\ n}{B^2}$$ Equation 61

$$fmep_{ring\ and\ gas} = \frac{(p_a - p_1)}{14.2}\frac{2.35\ S}{B^2}\left[0.088R_c + 0.182R_c^{\left(1.33-\left(0.121V_p/1000\right)\right)}\right] \quad \text{Equation 62}$$

The coefficients of the equations used for modeling the piston friction was defined in units of inches as M=Piston skirt length/bore, V_p=Mean piston speed (Ft/minute), B=Bore, and S=Stroke.Bishop defined the summation of his equations 51, 52, 53, 58, 59, 60, 61 and 62 as the total frictional losses.

Table 5 - Friction Coefficients (Bishop, 1964)

Coefficient	Value
K (Typical value for engines with babbit bearings)	1.76
K (Typical value for engines with micro babbit, copper-lead, or Al bearings)	0.85

Mass flow in/out cylinder:

Flow in and out of the combustion chamber was modeled using the general equations for flow past an orifice. The equations used for flow past the valve are from the doctoral dissertation of Jonathan Dawson (Dawson, 1998). The following equations determine the mass flow rate of fluid passing across an orifice. Dawson defined the following equations for un-choked flow.

$$\frac{p_{cyl,i}}{p_m} > \left[\frac{2}{\gamma+1}\right]^{\gamma/\gamma-1} \quad \text{Equation 63}$$

$$\dot{m} = \frac{C_D A_{valve} p_m}{\sqrt{RT}}\left(\frac{p_{cyl,i}}{p_m}\right)^{1/\gamma}\left\{\frac{2\gamma}{\gamma-1}\left[1-\left(\frac{p_{cyl,i}}{p_m}\right)^{\gamma-1/\gamma}\right]\right\}^{1/2} \quad \text{Equation 64}$$

Dawson defined the following equations for choked flow. This is standard practice since the high pressure difference across the orifice leads to sonic throttling. The flow rate is no longer a function of pressure difference across the orifice.

$$\frac{p_{cyl,i}}{p_m} \leq \left[\frac{2}{\gamma+1}\right]^{\gamma/\gamma-1}$$ Equation 65

$$\dot{m} = \frac{C_D A_{valve} p_m}{\sqrt{RT}} (\gamma)^{1/2} \left\{\frac{2}{\gamma+1}\right\}^{\gamma+1/2(\gamma-1)}$$ Equation 66

To determine the effective area of flow a function for lift needed to be generated. An approximate function of the cam profile is the sine function over the lift duration. The function to define lift can be seen below. The final pressure when the intake valve closes is most important when modeling IMEP, variation in the lift profile does not critically affect results.

$$L = L_{MAX} * \sin\left((\emptyset - VO)\frac{\pi}{VD}\right)$$ Equation 67

With the lift function generated, the valve area could be determined. The minimum of the port and curtain area was used to determine the effective area. This method is routinely used and has been found to accurately approximate experimental results. When the valve initially opens the effective area of the valve is limited to the curtain area which is the area between the outside diameter of the valve and the valve seat. When this area becomes equal to the port area the flow no longer increases linearly. In actuality the transition of flow rates between the two areas is not a sharp change but smoothed.

$$A_{curtain} = L * \emptyset_{valve} * \pi$$ Equation 68

$$A_{port} = \frac{\pi}{4}\left(\emptyset_{valve}{}^2 - \emptyset_{valve,stem}{}^2\right)$$ Equation 69

Modeling:

Matlab was used to model the above equations. The code developed by Buttsworth was used as a starting point. Buttsworth used variations of routines developed by Olikara and Borman as well as routines by Ferguson. The chemical combustion routine used by

Buttsworth use the reactant properties of air curve fitted from JANAF tables. The curves return the ratio of specific heats, enthalpy and entropy based on the temperature of the reactants. Buttsworth used two curve fitted coefficients "Gordon and McBride" and Chemkin, but found the results to be similar with insignificant differences. The functions provide data for 10 species CO_2, H_2O, N_2, O_2, CO, H_2, H, O, OH, and NO. The thermodynamic properties of the fuel were determined using curves given by Heywood. The curves given by Heywood also return ratio of specific heats, enthalpy and entropy. The model uses the results of the air and fuel data to determine the product composition using the FARG and ECP subroutines. These subroutines are Matlab versions of the original FORTRAN subroutines. FARG is used at lower temperatures and ECP is used at higher temperatures above 1000K. Buttsworth used the code from Ferguson to determine the pressure, temperature, work, heat loss, and enthalpy change during combustion. The Matlab function ode45 was used to solve the initial value ordinary differential equations presented by Ferguson. Ferguson split the combustion phases into functions for compression, combustion, and expansion. His model was expanded here to include phases for intake and exhaust so that losses from the pumping loop could be considered.

Chapter 4 Model Analysis

Sensitivity Analysis/Variation of Parameters

A Sensitivity analysis was carried out to determine which parameters had the greatest influence on IMEP. All parameters were individually increased by 10% to determine their influence. The results of the analysis can be seen below.

Table 6 - Sensitivity of parameters with respect to IMEP

Engine Geometry	**Value**	**Parameter +10%**	**% Var**
Bore	0.079	0.0869	0.044
Stroke	0.0836	0.09196	0.409
Compression Ratio	12.2	13.42	0.297

Engine Thermo Fluids Parameters	**Value**	**Parameter +10%**	**% Var**
Piston Blowby Constant	0.8	0.88	0.290
Tangential Velocity of Swirling Gasses	1	1.1	0.001
Squish Velocity	1	1.1	0.000
Residual Fraction	0.1	0.11	0.972
Equivalence Ratio	0.66	0.726	7.893
Start of Burn	-6	-7	0.965
Burn Duration	70	77	3.994
Engine Speed	1800	1980	0.277
Unburned Zone Heat Transfer Coefficient/Weighting	0.05	0.055	0.378
Burned Zone Heat Transfer Coefficient/Weighting	0.09	0.099	0.411
Engine Surface Temperature	1450	1595	2.938

Initial Conditions in Combustion Chamber at BDC	**Value**	**Parameter +10%**	**% Var**
P1	101325	91193	35.376
T1	330	363	21.456

The parameters with the greatest influence on IMEP were pressure, temperature, engine surface temperature, burn duration, start of burn, equivalence ratio, and residual

fraction. Squish and swirl velocities when varied by small amounts have little influence in the model. Their increases velocities attribute only to heat losses. The increased mixing from the induced turbulence does not decrease the time losses that would be realized from the shortened burn duration.

Comparison of Wiebe functions

Previously in Figure 22 the variation in the rate of burn between a Wiebe function based on the cosine function and an exponential function were evaluated. The previous results were based on a cosine based Wiebe function. The variation between the cosine and exponential versions will be explored. The results show that difference in Wiebe function between equations 10 and 11 is minimal. The results vary by less than 1%.

Table 7 - Variation of IMEP from Wiebe Function

	IMEP
Eqn. 10 (Exponential)	900510
Eqn. 11 (Cos)	908770
Difference	0.92%

Variation in Start of Burn and duration

The IMEP is greatly affected by the start of burning and the duration. The following figure shows the variation in IMEP with the start of burning. As would be expected both figures show the highest IMEP when the middle of the burn is at TDC. Since this program assumes burn duration and start of burn to be independent parameters, the highest IMEP would occur when combustion occurs instantaneously at TDC. The approximate values of each of these parameters will be determined from the experimental results.

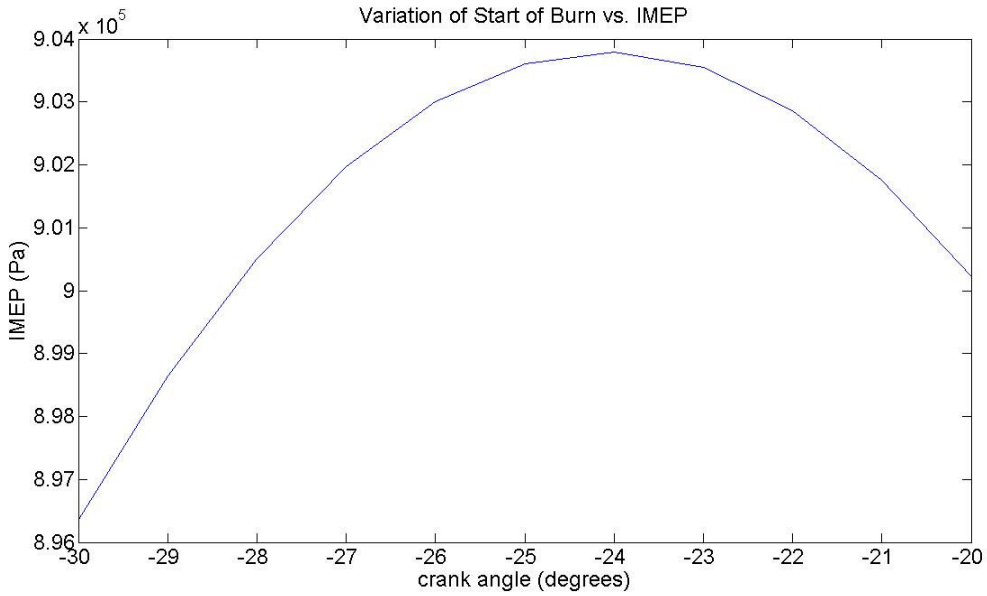

Figure 23 - Variation of Start of Burn vs. IMEP (Burn Duration 54°)

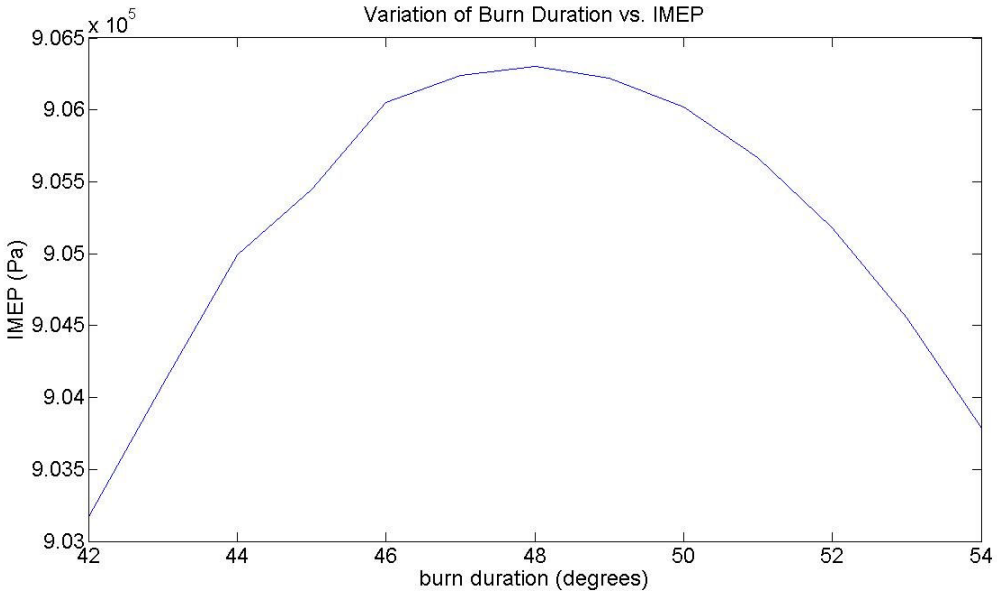

Figure 24 - Variation of Burn Duration vs. IMEP (Start of Burn -24°)

Residuals

Residuals have a large impact on IMEP. The residual fraction was incrementally increased and the resultant IMEP is shown in the following figure. The model predicted that IMEP would linearly decrease with increasing residual fraction. The equation of the

line was found to be ($IMEP = -972{,}064.04 * Residual\ fraction + 1{,}005{,}234$). When the predicted line was extrapolated to zero, the corresponding residual fraction was approximately 1.03; this would suggest that there is some error in the model. Since the error is small here it is attributable to round-off. However in the actual engine if the residual fraction was increased the fuel to air ratio of the entire system would decrease since less fresh mixture was added at the start of each cycle.

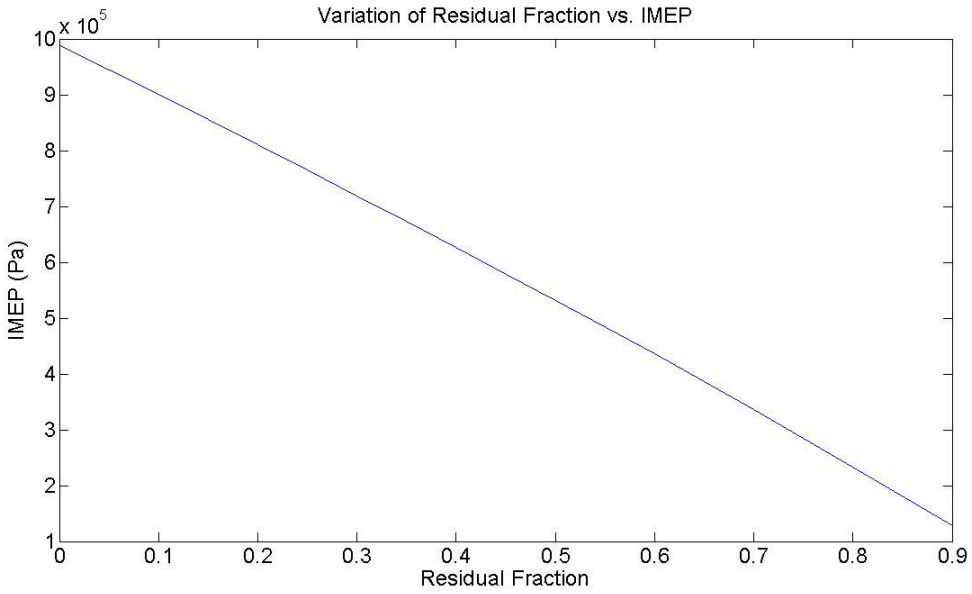

Figure 25 - Variation of Residual Fraction vs. IMEP

Pressure at the beginning of compression

The pressure at the beginning of compression at BDC was varied to find the effect on IMEP. This would correlate to opening or closing the throttle. The results of varying the pressure were found to affect IMEP linearly. The correlation can be seen in the next figure. As would be predicted the IMEP increased with increasing pressure at the start of compression. When more air is added to the combustion chamber there is a greater capacity available to combust. A linear relationship between IMEP and Pressure at BDC is to be expected.

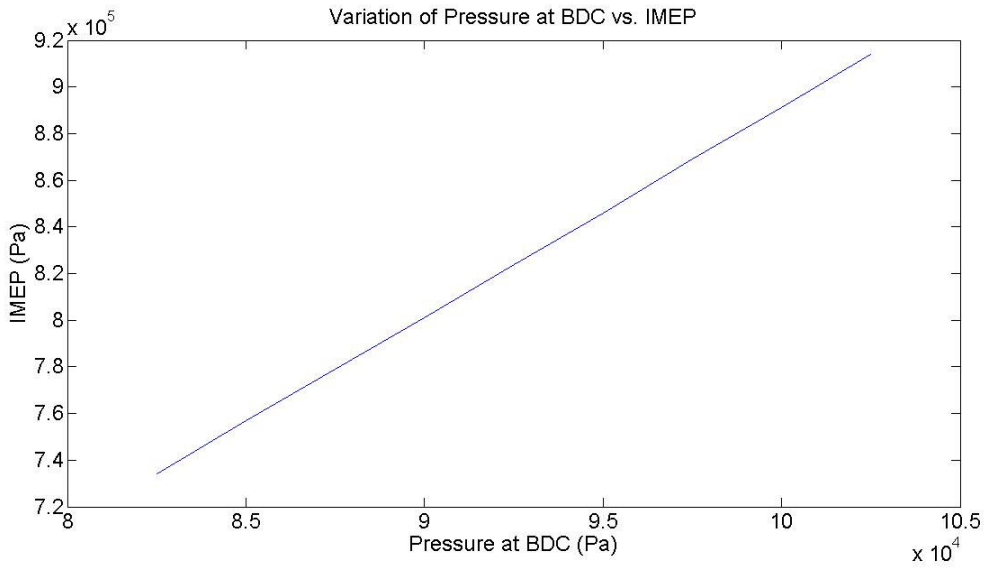

Figure 26 - Variation of Pressure at TDC vs. IMEP

Variation in heat loss from swirl and squish

The heat loss throughout the cycle can be seen below. During the intake and compression stroke the gas temperature is below the wall temperature of the gasses. It isn't until after combustion has initiated that the temperature of the gasses becomes higher than the wall temperature and heat flows out of the system. During expansion the gasses are at a high temperature for an extended period of time with a relatively high surface area.

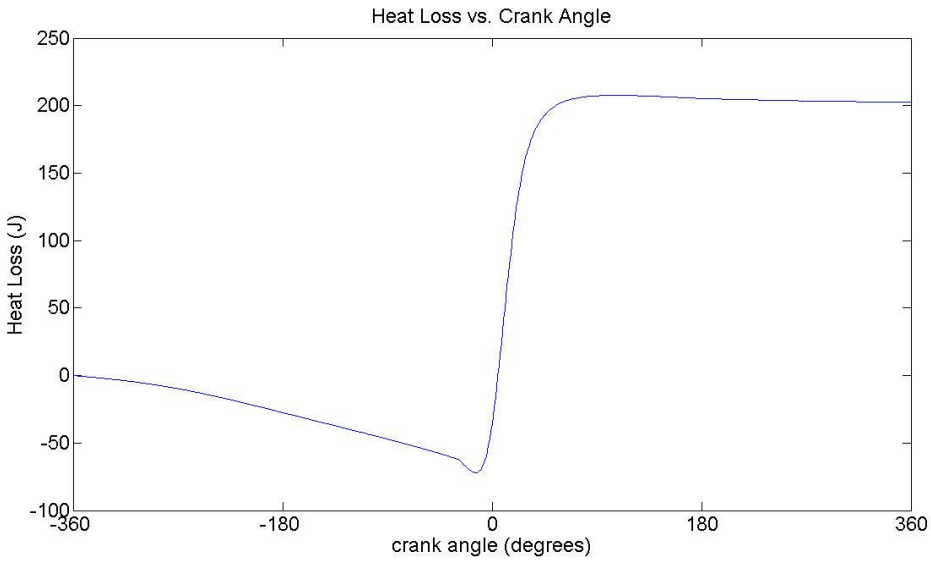

Figure 27 – Heat Loss vs. Crank Angle

Friction

The frictional losses for the Heywood and Sandoval and the Bishop models can be seen in the following bar graphs. The Bishop model was developed in 1964 and has much higher values for friction. The higher values are due to advances in ring design and piston advancements that are seen in newer engines. Advanced in piston ring technology have greatly reduced engine friction over the last 50 years. The total fMEP at 1800 RPM for the Bishop model is 180.2 kPA while the Heywood and Sandoval model predicted a fMEP of 103.6 kPA. The Bishop model predicted much higher PMEP than would be predicted by Heywood.

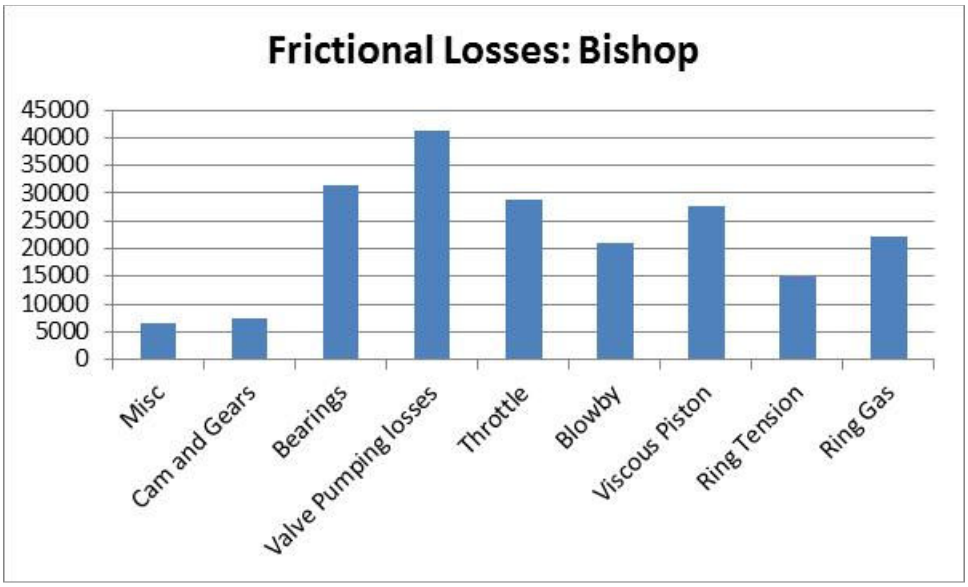

Figure 28 – Bishop Frictional Losses

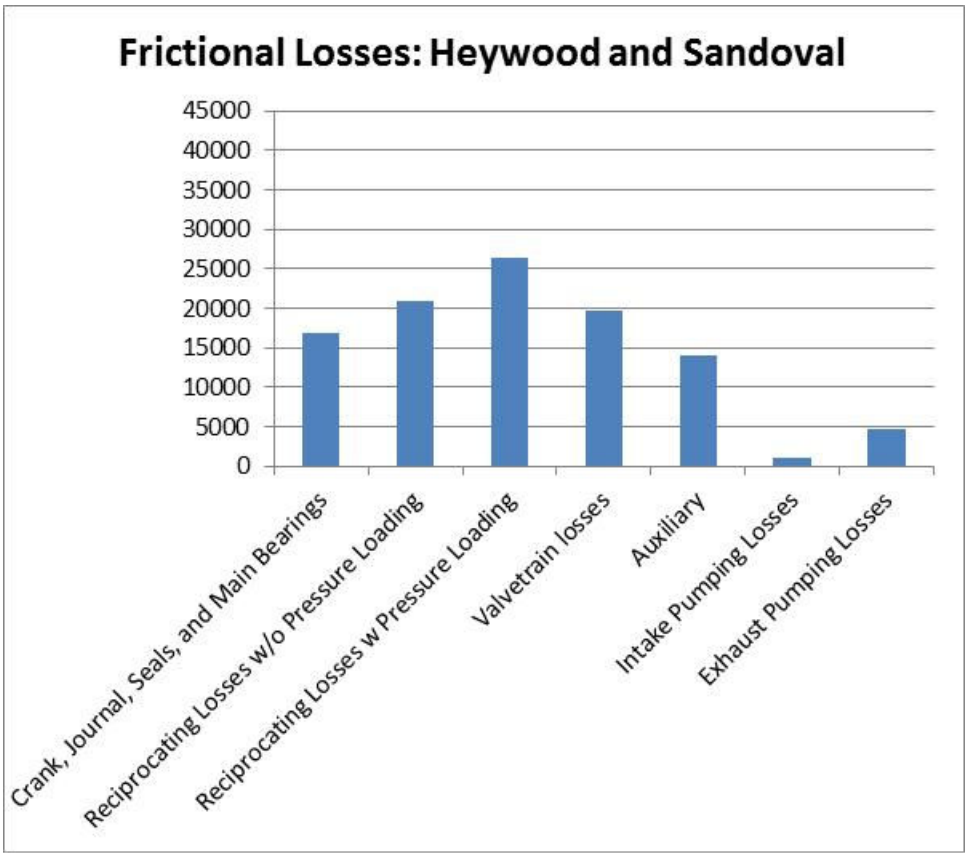

Figure 29 – Heywood and Sandoval Frictional Losses

A comparison of the two models shows that for most parts of the engine the Bishop model predicts much higher results. The only exception is for the auxiliary or miscellaneous friction when Bishop gave lower results. The Bishop model did not separate friction between bearing surfaces and valve train; no results were available to compare with the Heywood and Sandoval model. The explanation for the large difference in results is that frictional losses in engines have significantly decreased since publishing the Bishop paper.

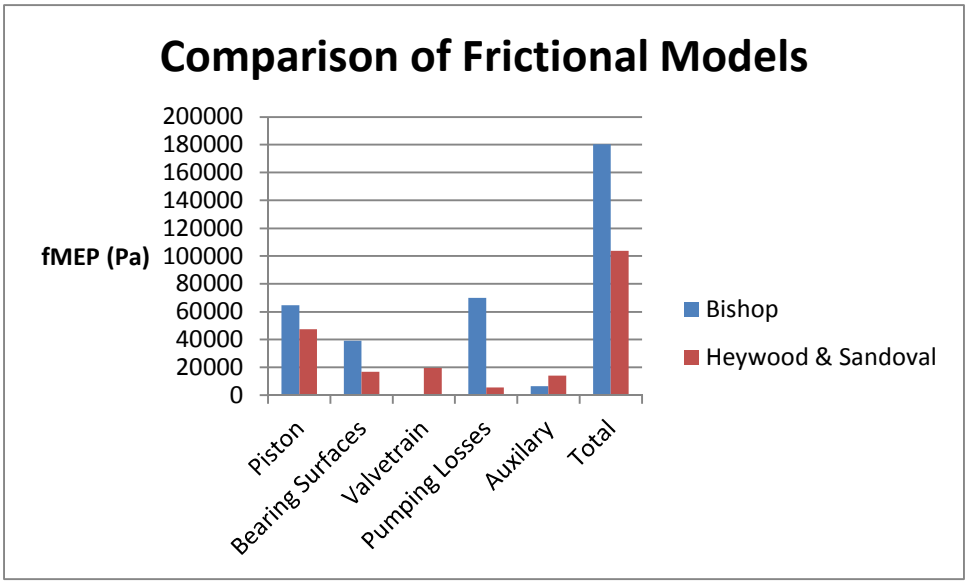

Figure 30 - Comparison of Heywood and Bishop Models

The parameters used for engine geometry can be seen in Table 8. The compression was determined using the engine geometry and the dead volume in the cylinder heads as well as the volume from the valve reliefs in the flat top pistons.

Table 8 – Engine Geometry Parameters

Parameter	Value	Units
Bore	0.079	m
Stroke	0.0836	m
Half Stroke to Rod Ratio (Stroke/(2*Connecting Rod Length)	0.308	m/m
Compression Ratio	12.2	

Table 9 - Intake/Exhaust Valve Parameters

Parameter	Value	Units
Discharge Coefficient for the Intake Valve	7	
Max Intake Lift	0.0096012	m
Opening of Intake Valve (IVO)	TDC (-360deg)	
Duration for Intake Valve to be Open (IVD)	180	deg
Intake Valve Diameter	0.0375	m
Intake Valve Stem Diameter	0.00635	m
Discharge Coefficient for the Exhaust Valve	7	
Max Exhaust Lift	0.0096012	m
Opening of Exhaust Valve (EVO)	BDC(180deg)	
Duration for Exhaust Valve to be Open (EVD)	180	deg
Exhaust Valve Diameter	0.032004	m
Exhaust Valve Stem Diameter	0.00635	m

Table 10 – Thermodynamic and Fluidic Parameters

Parameter	Value	Units
Piston Blowby Constant	0.8	1/s
Residual Fraction	0.1	
Fuel Type	Propane	N/A
Airscheme	GMcB	N/A
Equivalence Ratio	0.66	kg/kg
Start of Burn	-28	deg
Burn Duration	54	deg
Engine Speed	1800	RPM
Unburned Zone Heat Transfer Coefficient/Weighting	10	N/A
Burned Zone Heat Transfer Coefficient/Weighting	10	N/A
Engine Surface Temperature	450	K
Intake Temperature	299	K
Intake Pressure	80761.5	Pa
Exhaust Pressure	101325	Pa

Table 11 - Frictional Parameters

Parameter	Value	Units
Firing exhaust back pressure at 4000RPM	137895.1456	Pa
Bearing Information		
Journal Bearing Diameter	0.0499	m
Main Bearing Diameter	0.0399	m
Main Bearing Length	0.0176	m
Journal Bearing Length	0.0171	m
Number of Journal Bearings per Piston	1	
Number of Main Bearings per Cylinder	1.25	
Accessory Bearing Diameter	0.05	m
Accessory Bearing Length	0.02	m
Number of Cylinders	1	
Piston Information		
Piston Skirt Length	0.04826	m
Number of Rings per Cylinder (Compression + Oil Rings)	3	
Piston Roughness Constant	0.01	
Oil information		
Viscosity of Oil	10.8	cst
Viscosity of Oil at reference point	74.8	cst
Cam to Valve Frictional Losses Coefficients		
Frictional Losses in the Mixed Lubrication Regime	400	
Frictional Losses in Roller Contact	0	
Frictional Losses Oscillating Hydrodynamic Friction	0.2	
Frictional Losses Oscillating Mixed Lubrication Friction	21.4	

Chapter 5 Experimental Setup

The experimental data was collected in the University of Miami Internal Combustion engines lab. Three different cylinder head configurations were used for testing. The first generated 18.4% squish and generated low amounts of swirl. The second head also generated 18.4 % squish but generated high swirl. The third head generated extremely high swirl and 33.9% squish. All heads were based on the 1.3L head. Using the smaller head allowed for smaller port diameters which allowed for more swirl to be generated from the increased port velocity. The compression ratios used were 12.2:1 for the low swirl, and high swirl configurations. The super high swirl configuration used a compression ratio of 12.7:1. All configurations used flat top pistons, two valves per cylinder and a hemispherical combustion chamber.

Data was collected using a water brake Superflow dynamometer model D-516. The engine speed was collected using stroboscope to measure RPM of the crank. The stroboscope used was a AMETEK model Digistrobe III 1965. The timing and engine management was controlled using a Haltech E8 engine control unit. Measurements for fuel flow were measured using a Cox model 129-287 rotameter. The exhaust measurements were taken using thermocouples and an O_2 sensor. The flow rate of air entering at the intake was measure using a Meriam Laminar Flow element and incline manometers to measure the pressure. The laminar flow element is accurate to 100 CFM at 8" H_2O at the atmospheric conditions of 70°F and 29.92 in*Hg Abg. The information about the instrumentation can be seen in the following table.

Table 12 - Data Collection Instrumentation

Measurement Device Description	Manufacturer	Model	Accuracy and Range
Dynamometer	Superflow	D-516	±.2% Reading
Stroboscope	Ametek	Digistrobe III 1965	±1% Reading
ECU	Haltech	E8	
Thermocouple	Omega	OMEGACLAD KMQXL-032G-6	
O_2 Sensor	Innovative	LM-2 Air/Fuel Ratio Meter	
Laminar Flow Element	Meriam	50 MC2-2P	±.65% Reading, 0-100 CFM
Incline Manometer	Meriam	40OHE35WM	
Ambient Pressure Gauge	Oakton	Aneroid Manometer	

During testing the engine was allowed to warm up to operating temperature before measurements we taken. When the oil and coolant temperatures became stable the engine was considered to be at operating condition. The initial conditions were around 25° spark advance and 1800 RPM. Since the engine was intended to be used as a generator engine at constant speed the removal of engine speed as a parameter of variation, simplified testing. The load, spark advance, throttle, and air-fuel ratio were all varied to determine the maximum power and BTE for each configuration.

The following three tables give experimental data collected for the three configurations. The spark advance for each equivalence ratio varied until the highest output was found.

Table 13 - Low Swirl Experimental Data

Torque (N*m)	27.39	27.25	27.12
RPM	1800	1800	1800
Lambda	1.25	1.32	1.16
Spark Advance	41	45	37
Temperature Exhaust (K)	815	805	840
Manifold Pressure (Pa)	39302	41715	37233

Table 14 - High Swirl Experimental Data

Torque (N*m)	25.76	27.52	27.79
RPM	1800	1800	1800
Lambda	1.25	1.41	1.44
Spark Advance	32	40	42
Temperature Exhaust (K)	816	780	773
Manifold Pressure (Pa)	39302	42404	42749

Table 15- Super High Swirl Experimental Data

Torque (N*m)	27.31	28.07	28.47	28.74
RPM	1807	1780	1774	1813
Lambda	1.26	1.51	1.60	1.66
Spark Advance	24	30	38	45
Temperature Exhaust (K)	788	740	721	712
Manifold Pressure (Pa)	42641	48533	50564	52258

Chapter 6 Comparison of Results

Comparison Experimental/Theoretical

The following section provides a comparison of experimental and theoretical results. Without the aid of a P-V Diagram the duration of combustion and the ignition delay are unknown. In this case the duration was assumed to be equal to the spark advance. To determine the start of combustion, the start of combustion was varied until the highest IMEP was found. Three different configurations were considered. The three configurations tested were no swirl, high swirl and super high swirl. The differing characteristics of each configuration are given in Table 16. Data was collected for loads around 27 N*m (~20 ft*lb).

Table 16- Configuration Characteristics

Configuration	Squish	Swirl Ratio	Compression Ratio
Low Swirl	18.4%	0.38	12.2:1
High Swirl	18.4%	1.5	12.2:1
Super High Swirl	33.9%	3.2	12.7:1

The first configuration examined was the low swirl head. The results can be seen in Table 17. The experimental and theoretical BTE never varied by more than 1.2% for any load. The FMEP remained relatively constant since the only variable changed between different loads was intake manifold pressure. FMEP varied from 67160 Pa to 68624 Pa. The highest BMEP and BTE efficiency was found at 36.9 N*m which had an experimental BTE of 24.2% and a theoretical BTE of 25.4%.

Table 17 - Low Swirl Engine Configuration Results

Torque (N*m)	37.1	36.9	36.8
Lambda	1.25	1.32	1.16
Duration	41	45	37
Start Combustion	-12	-16	-9
Manifold Pressure (Pa)	39302	41715	37233
Heat Transfer Weighting Coef.	0.130	0.130	0.130
RPM	1800	1800	1800
IMEP (Pa)	348840	356940	349360
FMEP (Pa)	68083	68624	67160
PMEP (Pa)	62055	59642	64124
BMEP (Pa)	218702	228674	218077
Heat Loss in Combustion Chamber (J)	73	71	75
Heat Loss in Exhaust Port (J)	75	76	78
Heat Loss to Water Jacket (J)	148	147	153
Heat Loss in Exhaust Gases (J)	147	151	149
Heat Loss in Exhaust Gasses after Exhaust Port	68	72	67
Total Heat Losses (J)	220	223	223
Heat Loss in Combustion Chamber (%)	20.0%	19.3%	20.0%
Heat loss to Water Jacket (%)	40.5%	39.8%	41.0%
Heat Loss in Exhaust Gasses (%)	40.1%	41.0%	39.9%
Heat Loss in Exhaust Gasses after Exhaust Port (%)	18.7%	19.5%	18.0%
Total Heat Losses (%)	60.2%	60.3%	59.9%
ITE - Model	39.0%	39.6%	38.4%
BTE - Model	24.5%	25.4%	24.0%
BTE - Experimental	24.3%	24.2%	24.3%
Temperature of Exhaust Exiting the Combustion Chamber (K)	1236	1206	1298
Temperature of Exhaust After Exhaust Port (K)	784	778	800
Temperature of Exhaust After Exhaust Port Experimental (K)	815	805	840

The high swirl head results can be seen in Table 18. The theoretical and experimental BTE do not vary by more than 1%. Similar to the no swirl head the FMEP did not vary significantly. FMEP varied from 67836 Pa to 68961 Pa. The highest BTE

was at the highest load of 37.7 N*m. At this load the experimental BTE was 25.4% and the theoretical BTE was 26.2%. The theoretical BMEP was 221422 Pa.

Table 18 – High Swirl Engine Configuration Results

Torque (N*m)	34.9	37.3	37.7
Lambda	1.25	1.41	1.44
Duration	32	40	42
Start Combustion	-4	-13	-15
Manifold Pressure (Pa)	39302	42404	42749
Heat Transfer Weighting Coef.	0.108	0.108	0.108
RPM	1800	1800	1800
IMEP (Pa)	357660	352770	348990
FMEP (Pa)	67836	68849	68961
PMEP (Pa)	62055	58952	58608
BMEP (Pa)	227769	224969	221422
Heat Loss in Combustion Chamber (J)	60	60	59
Heat Loss in Exhaust Port (J)	81	74	72
Heat Loss to Water Jacket (J)	142	134	131
Heat Loss in Exhaust Gases (J)	157	149	148
Heat Loss in Exhaust Gasses after Exhaust Port	71	72	72
Total Heat Losses (J)	217	209	206
Heat Loss in Combustion Chamber (%)	16.4%	17.1%	17.0%
Heat loss to Water Jacket (%)	38.6%	38.0%	37.8%
Heat Loss in Exhaust Gasses (%)	42.7%	42.4%	42.6%
Heat Loss in Exhaust Gasses after Exhaust Port (%)	19.5%	20.4%	20.6%
Total Heat Losses (%)	59.1%	59.5%	59.5%
ITE - Model	40.0%	41.1%	41.2%
BTE - Model	25.5%	26.2%	26.2%
BTE - Experimental	25.4%	25.2%	25.4%
Temperature of Exhaust Exiting the Combustion Chamber (K)	1293	1180	1164
Temperature of Exhaust After Exhaust Port (K)	803	770	765
Temperature of Exhaust After Exhaust Port Experimental (K)	816	780	773

Table 19 – Super High Swirl Engine Configuration Results

Torque (N*m)	37.0	38.0	38.6	39.0
Lambda	1.26	1.51	1.60	1.66
Duration	24	30	38	45
Start Combustion	2	-5	-11	-17
Manifold Pressure (Pa)	42641	48533	50564	52258
Heat Transfer Weighting Coef.	0.108	0.108	0.108	0.108
RPM	1807	1780	1774	1813
IMEP (Pa)	361770	359330	357640	362190
FMEP (Pa)	69579	71642	72348	72859
PMEP (Pa)	58716	52824	50792	49099
BMEP (Pa)	233475	234864	234500	240232
Heat Loss in Combustion Chamber (J)	60	63	62	60
Heat Loss in Exhaust Port (J)	82	71	68	69
Heat Loss to Water Jacket (J)	142	134	131	128
Heat Loss in Exhaust Gases (J)	158	149	148	150
Heat Loss in Exhaust Gasses after Exhaust Port	72	74	75	77
Total Heat Losses (J)	218	212	210	210
Heat Loss in Combustion Chamber (%)	16.3%	17.8%	17.8%	17.0%
Heat loss to Water Jacket (%)	38.4%	37.7%	37.3%	36.6%
Heat Loss in Exhaust Gasses (%)	42.7%	41.8%	42.1%	42.8%
Heat Loss in Exhaust Gasses after Exhaust Port (%)	19.6%	20.9%	21.4%	22.0%
Total Heat Losses (%)	59.0%	59.7%	59.9%	59.8%
ITE - Model	40.3%	41.0%	41.2%	42.6%
BTE - Model	26.0%	26.8%	27.0%	28.3%
BTE - Experimental	26.1%	24.6%	27.1%	27.4%
Temperature of Exhaust Exiting the Combustion Chamber (K)	1288	1115	1076	1062
Temperature of Exhaust After Exhaust Port (K)	803	751	739	735
Temperature of Exhaust After Exhaust Port Experimental (K)	788	740	721	712

The Super high Swirl Engine configuration results can be seen in Table 19. The variation between the theoretical and experimental BTE was less than 2.2%. The FMEP varied between 69579 Pa and 72859 Pa. The highest BTE and BMEP was at the load of

39.0 N*m. The experimental BTE was 27.4% and the theoretical was 28.3%. The theoretical BMEP was 240232 Pa.

Analysis of Heat Losses:

Figure 31 gives a comparison of the instantaneous heat transfer coefficient for λ=1.25. Low swirl has the highest instantaneous heat transfer coefficient out of the three configurations and is maintained over the longest duration. The increased gas velocities due to squish are evident in the Super High Swirl configuration. The High Swirl engine has the lowest peak heat transfer coefficient. Figure 32 shows the instantaneous heat transfer coefficient for the High Swirl and Super High Swirl engine configurations. The low swirl engine was not able to run at these lean mixtures since there was not adequate turbulence to increase the flame speed to burn the mixture efficiently. Here there is a higher instantaneous heat transfer coefficient in the Super High Swirl engine.

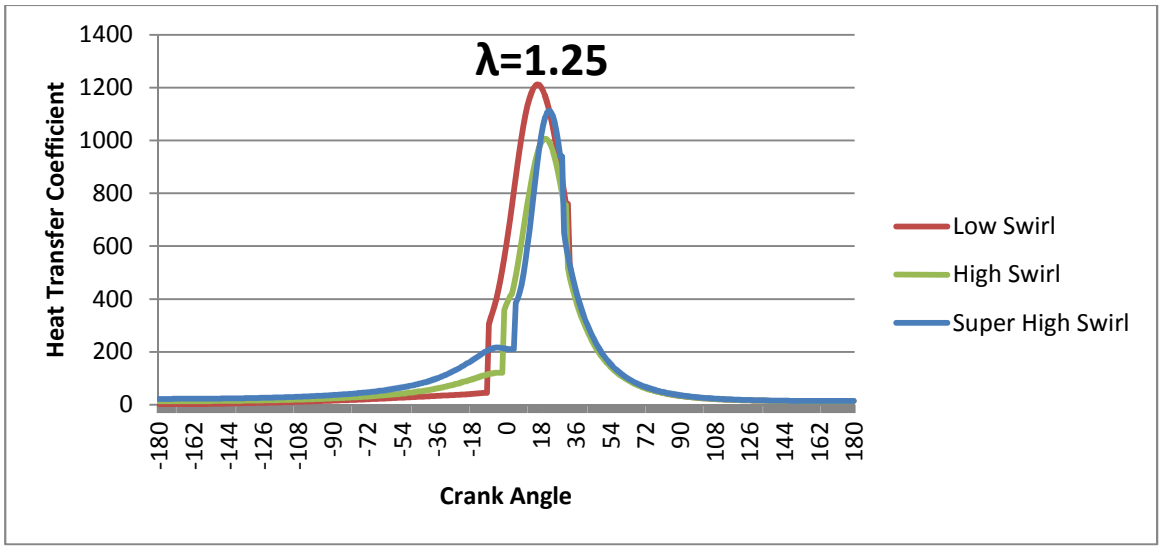

Figure 31 – λ=1.25 Instantaneous Heat Transfer Coefficient

Figure 33 shows the leanest mixtures run at this load. It should be noted that the Super High Swirl engine instantaneous heat transfer coefficients only varied slightly in peak amplitude and overall shape across varying equivalence ratios.

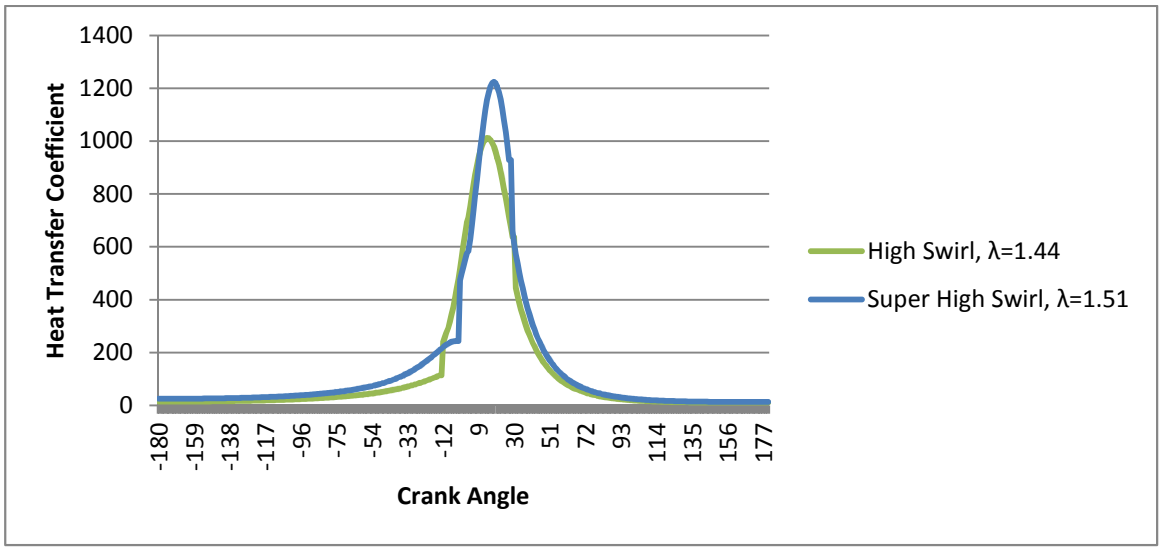

Figure 32 – Instantaneous Heat Transfer Coefficient

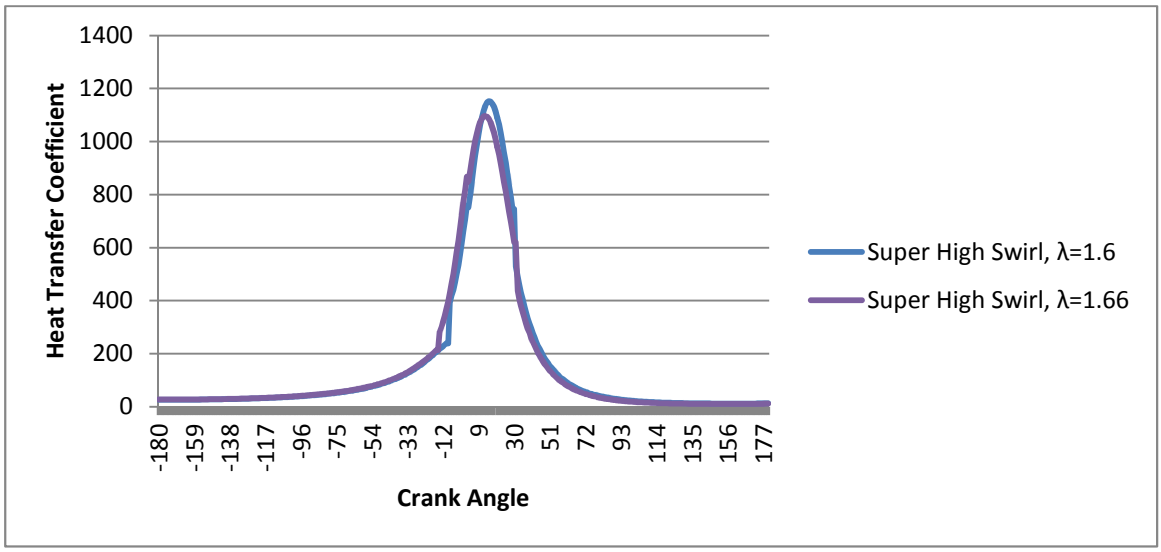

Figure 33 – Super High Swirl Instantaneous Heat Transfer Coefficient

The overall gas velocities for all three engine configurations can be seen in Figure 34**.** The Super High Swirl has noticeably higher gas velocities prior to combustion than any of the others and the rise in velocity is more prominent than the others. There is a

peak from the gasses being squished; whereas the High Swirl and Low Swirl engines only have a slight change in slope near where squish occurs. Figure 35 shows only the squish velocities for each engine configuration. Since the Low Swirl and High Swirl configurations both have the same squish area, their velocities are the same. The increased squish area of the Super High Swirl configuration more than doubles the peak squish velocity.

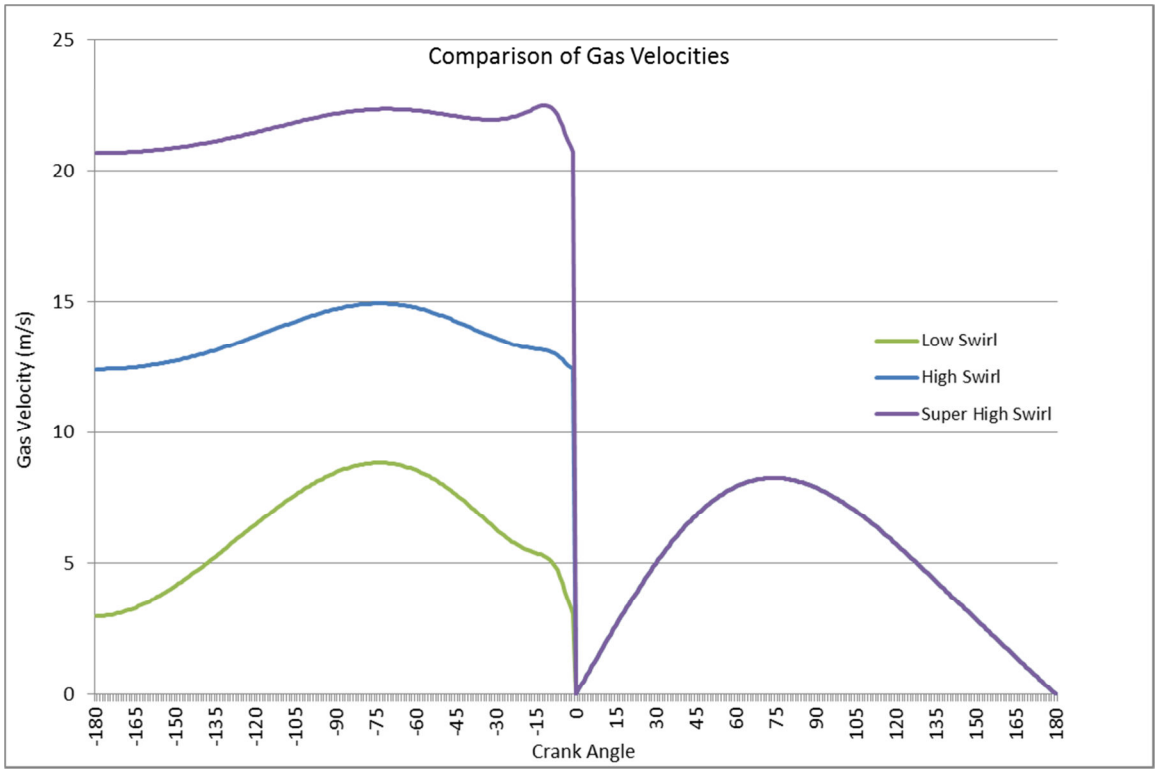

Figure 34 - Comparison of Gas Velocities

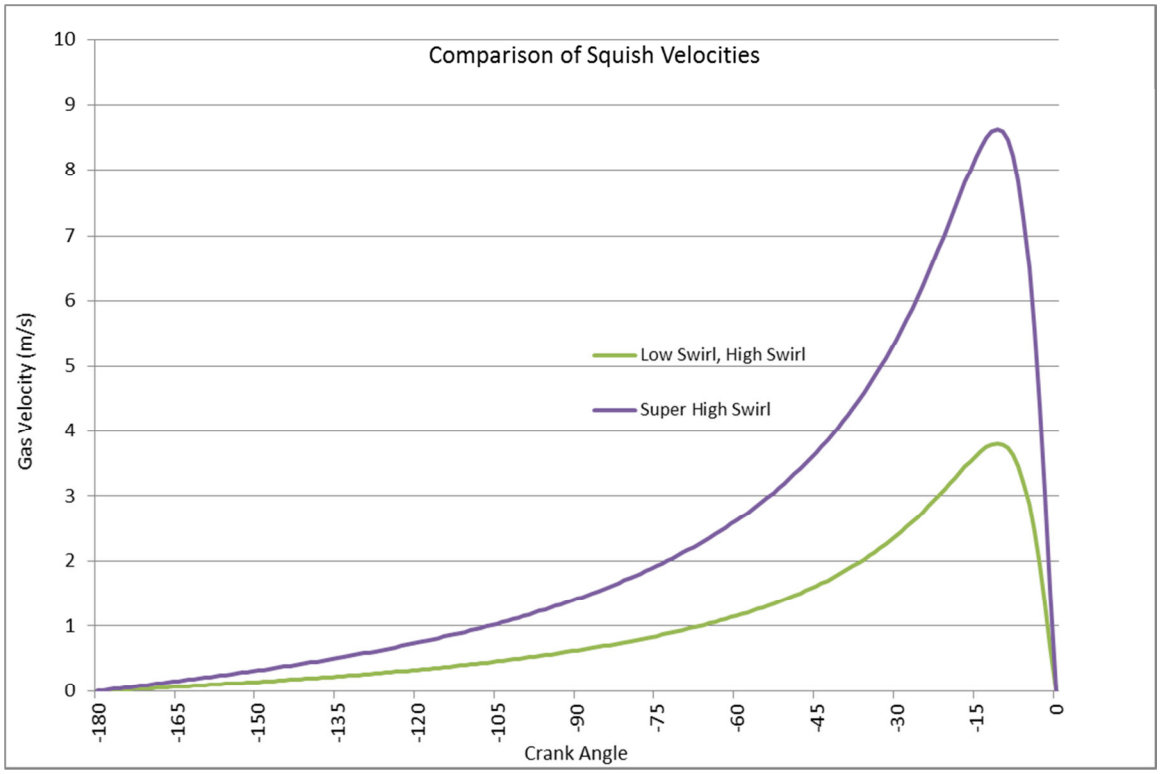

Figure 35 - Comparison of Squish Gas Velocities

The following Figure shows the Air-Fuel ratio compared to total heat losses. The plot shows that the higher swirl ratios were able to burn leaner mixtures and turn more of the heat from fuel into useable energy. Heat losses for each configuration were seen to increase at leaner mixtures due to the increased time losses.

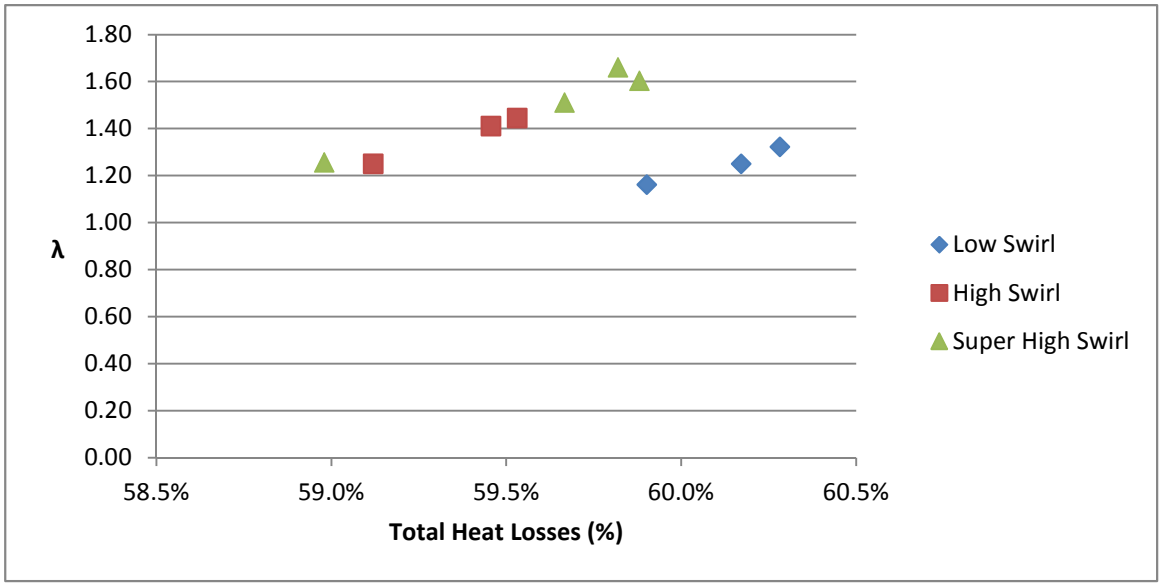

Figure 36 - Comparison of Heat Losses and Air-Fuel Ratio

Chapter 7 Conclusion

1. From the experimental testing it is evident that the squish areas and swirl ratios used in automobile engines designed for gasoline operation are not sufficient for lean burn LPG fueled genset engines.
2. Simply increasing compression ratios to 12.2:1 or 12.7:1 on stock gasoline engines designed for stoichiometric operation does not increase flame speed adequately for lean burn LPG genset engines.
3. When increasing the swirl ratio and squish area appreciably and running rich mixtures of LPG ($\lambda \leq 1.25$) large heat losses occur.
4. The improvements in BTE do not require the used of fuel injection or any other types of costly technology. The use of a pre-chamber between the gas mixer and intake manifold runners can provide sufficient mixing to virtually eliminate cylinder to cylinder fuel distribution problems and still require only 2.8 kPa intake manifold vacuum at 1800 rpm wide-open throttle.
5. These improvements do not require using welding to add material to any engine component but do require CNC'd combustion chambers.
6. Valve spring pressure used in automobile gasoline engines can be reduced at least 50% at all valve lifts without adverse effects.
7. The changes in valve springs reduced FMEP approximately 3 to 4 kPa at 1800 rpm for this application.
8. It is possible to rebuild a 1.6L genset engine using nonstandard but similar cost parts producing an increase in BTE to in excess of 37.0%. This represents an

improvement in fuel consumption of over 30% compared to the engine rebuilt utilizing standard parts.

9. The computer model of the three configurations of the engine evolution showed the third engine approaching optimization. This can be seen since the heat losses to the combustion chamber for the three engines were reduced from 20.1% (LS) to 16.7% (HS) and to 16.3% (SHS). Further increases in mixture turbulence will not likely result in decreased heat losses to the combustion chamber.

References

Baker, P. and Watson, H., (2005). "MPI Air/Fuel Mixing for Gaseous and Liquid LPG," SAE Technical Paper 2005-01-0246.

Bishop, I. (1964). “Effect on Friction and Economy”, SAE Technical Paper 640807.

Buttsworth, David R. (2002). "Spark Ignition Internal Combustion Engine Modeling Using Matlab." Web. <http://www.usg.edu.au/users/buttswod/>.

Dawson, Jonathan. (1998). “An Experimental and Computational Study of Internal Combustion Engine Modeling for Controls Oriented Research”(Doctoral Dissertation), (pg 75-79), ProQuest Dissertations and Theses Database. (UMI Number 9833964)

Ferguson,C . (1986). Internal Combustion Engines: Applied Thermosciences. New York: Wiley.

Gordon, S. and McBride, B. (1971) “Computer Program for Calculation of Complex Chemical Equilibrium Composition. Rocket Performance, Incident and Reflected Shocks, and Chapman-Jouguet Detonations”, NASA publication SP-273.

Heywood, J. (1988). Internal Combustion Engine Fundamentals. New York: McGraw-Hill.

Heywood, J. and Sandoval, D. (2003). “An Improved Friction Model for Spark-Ignition Engines” SAE Technical 2003-01-0725

Huffman, David G. “Using the ideal gas law and heat release models to demonstrate timing in spark and compression ignition engines” International Journal of Mechanical Engineering Education, Vol 28 No 4, 1999.

Kee, R., Rupley, F. and Miller, J.(1991). “The Chemkin Thermodynamic Data Base”. Sandia Reports SAND87-8215B.

Li, L., Wang, Z., Wang, H., Deng, B. et al., (2002). "A Study of LPG Lean Burn for a Small SI Engine," SAE Technical Paper 2002-01-2844.

Meisner, Steve and Sorenson, S.C. (1986). “Computer Simulation of Intake and Exhaust Manifold Flow and Heat Transfer”, SAE Paper 860242

Mizushima, N., Sato, S., Ogawa, Y., Yamamoto, T. et al., (2009). "Combustion Characteristics and Performance Increase of an LPG-SI Engine with Liquid Fuel Injection System," SAE Technical Paper 2009-01-2785.

Obert, Edward (1973). Internal Combustion Engines and Air Pollution. Michigan: International Textbook Co.

Olikara, Cherian and Borman, Gary L. (1975). “A Computer Program for Calculating Properties of Equilibrium Combustion Products with Some Applications to I.C. Engines.” SAE Technical 750468.

Quader, A.,(1974). "Lean Combustion and the Misfire Limit in Spark Ignition Engines," SAE Technical Paper 741055.

Sandoval, Daniel and Heywood, John. (2003). “An Improved Friction Model for Spark-Ignition Engines”, SAE Technical 2003-01-0725.

Thring, R. and Overington, M., (1982). "Gasoline Engine Combustion - The High Ratso Compact Chamber," SAE Technical Paper 820166.

Woschni, G. (1967). “A Universally Applicable Equation for the Instantaneous Heat Transfer Coefficient in the Internal Combustion Engine”, SAE Technical 670931.

Appendix

A.1

	Compression Ratio	Squish	Averaged Swirl Ratio	Valve Spring Force N		Intake Valve Closing ° ABDC	Cam Duration ° @ .086cm lift	Valve Max lift	
				Valve Closed	Valve Open			Intake (cm)	Exhaust (cm)
Engine 1 (NS)	12.2	18.4%	0.38	187	512	24.5	206/206	0.856	0.859
Engine 2 (HS)	12.2	18.4%	1.50	187	516	24.5	206/206	0.856	0.859
Engine 3 (SHS)	12.7	33.9%	3.20	107	254	18.5	188/188	0.861	0.859